LAMPIRAN

Luaran - 1

Status ***Published*** penelitian HMSIW C-band pada 19 Maret di Journal JoCM dengan judul "*Bandwidth Enhancement of HMSIW Antenna using Half-Octagonal Ring Slot*"

https://www.jocm.us/show-317-2058-1.html

Index Scopus Q3

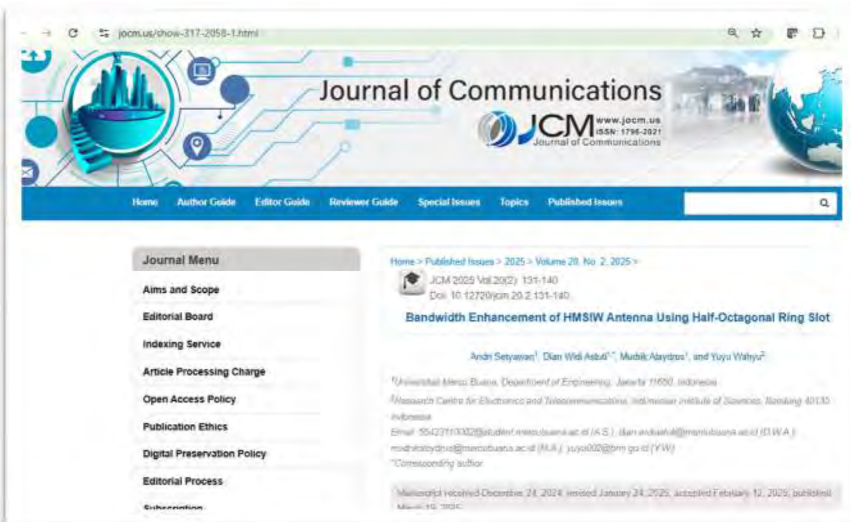

Luaran – 2

Status ***Published*** Penelitian HMSIW S-band pada 26 Mei 2025 di Jurnal PIER dengan judul "*Half-mode Substrate Integrated Waveguide Cavity Slot Antenna with Half-octagonal Ring Slot at S-band Frequency*"

https://www.jpier.org/PIERC/pier.php?paper=25031301

Index Scopus Q3

Luaran – 3

Hak Kekayaan Intelektual (HKI), Surat Pencatatan Ciptaan Poster dengan Judul : Antena *Half-mode* SIW pada Frekuensi S-band dengan Slot cincin setengah segi delapan untuk Peningkatan *Bandwidth*

SURAT PENCATATAN CIPTAAN

Dalam rangka pelindungan ciptaan di bidang ilmu pengetahuan, seni dan sastra berdasarkan Undang-Undang Nomor 28 Tahun 2014 tentang Hak Cipta, dengan ini menerangkan:

Nomor dan tanggal permohonan	:	EC002024256284, 19 Desember 2024
Pencipta		
Nama	:	**Dr. Dian Widi Astuti, ST, MT dan Andri Setyawan**
Alamat	:	Jalan H. Marjuki No. 9 Rt 002 Rw 015, Kec. Larangan, Kota Tangerang, Banten , Larangan, Tangerang, Banten, 15154
Kewarganegaraan	:	Indonesia
Pemegang Hak Cipta		
Nama	:	**Universitas Mercu Buana**
Alamat	:	Jl. Meruya Selatan No.1, RT.4/RW.1, Joglo, Kec. Kembangan, Kota Jakarta Barat, Daerah Khusus Ibukota Jakarta 11650, Kembangan, Jakarta Barat, Dki Jakarta 11650
Kewarganegaraan	:	Indonesia
Jenis Ciptaan	:	**Poster**
Judul Ciptaan	:	**Antena Half-mode SIW Pada Frekuensi S-Band Dengan Slot Cincin Setengah Segi Delapan Untuk Peningkatan Bandwidth**
Tanggal dan tempat diumumkan untuk pertama kali di wilayah Indonesia atau di luar wilayah Indonesia	:	19 Desember 2024, di Jakarta Barat
Jangka waktu pelindungan	:	Berlaku selama hidup Pencipta dan terus berlangsung selama 70 (tujuh puluh) tahun setelah Pencipta meninggal dunia, terhitung mulai tanggal 1 Januari tahun berikutnya.
Nomor pencatatan	:	000828716

adalah benar berdasarkan keterangan yang diberikan oleh Pemohon.
Surat Pencatatan Hak Cipta atau produk Hak terkait ini sesuai dengan Pasal 72 Undang-Undang Nomor 28 Tahun 2014 tentang Hak Cipta.

Bandwidth Enhancement of HMSIW Antenna Using Half-Octagonal Ring Slot

Andri Setyawan [1], Dian Widi Astuti [1,*], Mudrik Alaydrus [1], and Yuyu Wahyu [2]

[1] Universitas Mercu Buana, Department of Engineering, Jakarta 11650, Indonesia
[2] Research Centre for Electronics and Telecommunications, Indonesian Institute of Sciences, Bandung 40135, Indonesia
Email: 55423110002@student.mercubuana.ac.id (A.S.); dian.widiastuti@mercubuana.ac.id (D.W.A.); mudrikalaydrus@mercubuana.ac.id (M.A.), yuyu002@brin.go.id (Y.W.)
*Corresponding author

***Abstract*—This paper presents the design, simulation, fabrication, and measurement of a Half-Mode Substrate Integrated Waveguide (HMSIW) cavity slot antenna with a half-octagonal ring slot structure, operating in the C-band frequency range. The primary objective is to enhance impedance bandwidth while achieving significant miniaturization compared to conventional Substrate Integrated Waveguide (SIW) antennas. Simulated results demonstrate an impedance bandwidth of 18%, covering the frequency range of 5.60 GHz to 6.71 GHz, with an S_{11} value consistently below −10 dB. Fabrication and experimental testing validate these findings, achieving a measured impedance bandwidth of 19.4% over the range of 5.82 GHz to 7.07 GHz. The antenna exhibits a dual-directional and linear radiation pattern, radiating energy in both forward and backward directions, with a simulated gain of 2.73 dBi. The HMSIW structure achieves a 50% size reduction compared to full-mode SIW designs. These features make the proposed antenna suitable for modern telecommunications applications within the C-band, where wide bandwidth, miniaturization, and reliable linear radiation performance are essential. This advancement provides a promising solution for systems requiring high efficiency and reduced form factor without compromising performance.**

***Keywords*—Half-Mode Substrate Integrated Waveguide (HMSIW) antenna, C-band, bandwidth enhancement, half octagonal ring slots, miniaturization**

I. INTRODUCTION

Substrate Integrated Waveguide (SIW) cavity-backed slot antennas have received considerable attention due to their unique combination of waveguide properties with planar structures. These antennas offer a low-profile, high-efficiency design suitable for modern wireless communication, radar, and body area network applications. Despite their advantages, traditional SIW antennas often face limitations, such as narrow impedance bandwidth and moderate gain. As a result, researchers have focused on various techniques to address these challenges and improve antenna performance.

Tu *et al.* [1] and Luo *et al.* [2] investigated SIW cavity-backed slot antennas with Grounded Coplanar Waveguide (GCPW) feeding and hybrid cavity modes. Their approaches resulted in bandwidth improvements ranging from 1.7% to 6.3%. However, the gain enhancements remained moderate, restricting their suitability for high-gain applications.

Razavi and Neshati [3] applied HMSIW techniques to develop circularly and linearly polarized antennas [4]. These designs provided compact, low-profile antennas with excellent polarization characteristics. However, the bandwidth enhancements were relatively modest, limiting their use in broadband systems. Structural modifications such as substrate removal and slot shape alterations have proven effective for bandwidth enhancement. Yun *et al.* [5] employed substrate removal under the slot to improve bandwidth and efficiency. Mbaye *et al.* [6] and Tao *et al.* [7] employed dual-slot and bow-tie slot configurations, achieving bandwidths of 8.5% and 9.4%, respectively. Cheng *et al.* [8] introduced a modified dumbbell-shaped slot and utilized higher-order resonant modes to improve the bandwidth A hybrid approach combining patch and semi-circular SIW cavities also enhanced bandwidth, although at the cost of increased design complexity and modest gain improvements [9].

Slot geometry and cavity modifications have been employed to achieve multi-resonance and broader bandwidth. Yun *et al.* [10] introduced via-holes above the slot to create dual-resonance, which effectively enhanced bandwidth. Shi *et al.* [11] and Wu *et al.* [12] utilized shorting vias and unbalanced vias to achieve triple- and quad-resonance, respectively, improving the operational bandwidth. However, these techniques enhanced bandwidth, they introduced greater design complexity and demanded precise fabrication. Hybrid HMSIW cavity designs have shown significant potential for bandwidth enhancement [13]. Astuti *et al.* [14] developed hybrid HMSIW antennas incorporating multiple resonances, such as triple- and quad-resonance, to achieve broader bandwidth. Chaturvedi and Kumar [15] used epsilon-shaped and triangular slots to enhance HMSIW antenna bandwidth while maintaining a low profile [16]. However, the structural complexity of these designs posed challenges for practical fabrication.

Manuscript received December 24, 2024; revised January 24, 2025, accepted February 12, 2025; published March 19, 2025.

doi: 10.12720/jcm.20.2.131-140

Dash *et al.* [17] introduced a self-multiplexing SIW cavity-backed antenna for hexa-band operation, providing versatility for multi-band applications. However, its design was constrained to specific frequency bands, limiting its broader applicability. Defected Ground Structures (DGS) and Quarter-Mode SIW (QMSIW) techniques have also been used for bandwidth improvement. Astuti *et al.* [18] employed DGS to achieve hybrid resonance and a 14.31% bandwidth enhancement. Astuti *et al.* [19] developed dual-cavity QMSIW antennas for enhanced bandwidth, while Jin *et al.* [20] proposed compact QMSIW antennas with linear and circular polarization capabilities. Although effective, these methods often increased fabrication complexity and provided limited bandwidth improvements.

Qin *et al.* [21] developed frequency-reconfigurable SIW antennas for S-band and C-band applications, achieving bandwidths of 18 MHz and 322 MHz, respectively. However, the frequency tuning mechanism introduced design complexity and limited tuning range. Zhou and Yang [22] explored eighth-mode SIW antennas with dual-sense circular polarization, achieving a 10.5% bandwidth and a gain of 5.74 dBic. However, the bandwidth was still constrained for certain applications. Recently, Astuti *et al.* [23] proposed a broadband HMSIW antenna employing a semi-hexagonal ring slot design to achieve multi-resonance in X-band applications. This design achieved a measured fractional bandwidth of 34.46% (8.91–12.62 GHz) through triple-resonance mechanisms, significantly enhancing bandwidth without compromising compactness. However, the intricate design of the semi-hexagonal slot increased fabrication complexity, particularly for high-precision manufacturing. Similarly, Astuti *et al.* [24] introduced a broadband half-mode SIW cavity antenna using a semi-rectangular ring slot, achieving a fractional bandwidth of 32.05% (9.51–13.14 GHz). By merging TE_{101}, TE_{102}, and TE_{202} modes, this design ensured robust broadband performance while maintaining a low profile. Nevertheless, the reliance on mode-merging required meticulous optimization of slot parameters to achieve consistent results. These advancements demonstrate the potential of hybrid designs to balance bandwidth, gain, and structural simplicity, further advancing SIW antenna technology.

II. Design and Materials

The design of SIW cavity-backed slot antenna begins with a planar structure that integrates waveguide properties within a dielectric substrate. The antenna consists of a rectangular SIW cavity with metallic via-holes along its perimeter, which confine the electromagnetic energy and minimize leakage. A slot etched on the top layer of the substrate facilitates radiation, while the feeding mechanism employs a Grounded Coplanar Waveguide (GCPW) or microstrip line to ensure efficient energy transfer into the SIW cavity.

The substrate material used is Rogers RT/Duroid 5880, which has a thickness h of 1.575 mm, a tangent loss δ of 0.0009, and a dielectric relative permittivity ε_r of 2.2. This low-loss substrate is selected to maintain high efficiency and minimize dielectric losses, ensuring optimal performance in terms of bandwidth and efficiency. The combination of low-profile design and high-performance materials ensures that the antenna achieves the desired bandwidth and efficiency characteristics.

$$f_{mnp}^{SIW} = \frac{1}{\sqrt{\mu\epsilon}\,.\,2\pi}\sqrt{\left(\frac{m\pi}{L_{eff}^{SIW}}\right)^2 + \left(\frac{n\pi}{h}\right)^2 + \left(\frac{p\pi}{W_{eff}^{SIW}}\right)^2} \tag{1}$$

where $m = 1, 2\ldots$, $n = 1,2$, $p = 1, 2..$, and, $\varepsilon = \varepsilon_0.\varepsilon_r$, $\mu = \mu_0 \cdot \mu_r$ are the permittivity and permeability of the substrate, respectively. The equivalent length and width of the SIW cavity are critical parameters, calculated as functions of the resonator thickness, via diameter (D), and spacing between adjacent vias (V) [20].

$$\begin{cases} L_{eff}^{SIW} = L - 1.08\frac{D^2}{V} + 0.1\,\frac{D^2}{L} \\ W_{eff}^{SIW} = W - 1.08\frac{D^2}{V} + 0.1\frac{D^2}{W} \end{cases} \tag{2}$$

where, L and W represent the length and width of the rectangular SIW resonator, respectively. The condition $V < 0.25\lambda$ must be satisfied to ensure proper confinement of electromagnetic waves, where λ is the wavelength in the dielectric material. Double via-holes are aligned to make the SIW cavity functionally equivalent to a conventional metallic cavity.

The cavity dimensions were carefully adjusted to align with the operating frequency range, ensuring compatibility with C-band applications. The antenna was specifically designed to operate using TE_{101} and TE_{102} modes, with resonant frequencies calculated and listed in Table I.

Table II presents the dimensional parameters of the Ant-4, specified in millimeters, which are crucial for its structural and performance characteristics. These dimensions are optimized to ensure proper impedance matching and radiation efficiency, directly influencing the antenna's overall performance in the intended application.

The evolution of the SIW cavity-backed slot antenna design progresses through four stages: Ant-1, Ant-2, Ant-3, and the final design, Ant-4 as shown in Fig. 1. This iterative development focuses on enhancing bandwidth, gain, and overall efficiency while maintaining a low-profile structure.

TABLE I. Lists the Computed Series of TE Modes for the FMSIWs

m \ p	1	2	3	4	5
1	3.31	5.2393	7.41	9.66	11.95
2		6.63	8.45	10.48	12.62
3			9.94	11.72	13.66
4				13.25	15.00
5					16.57

TABLE II. Dimension of Ant-4 (Unit in Millimeters)

Parameter	*W*	*L*	*Lf*	*Wf*
Value	18	35	10	1.137
Parameter	*Ls*	*Ws*	*Hs*	*h*
Value	26.15	0.5	3.45	1.575
Parameter	*Lg*	*Wg*	*D*	*V*
Value	5.7	0.4	1	1.5

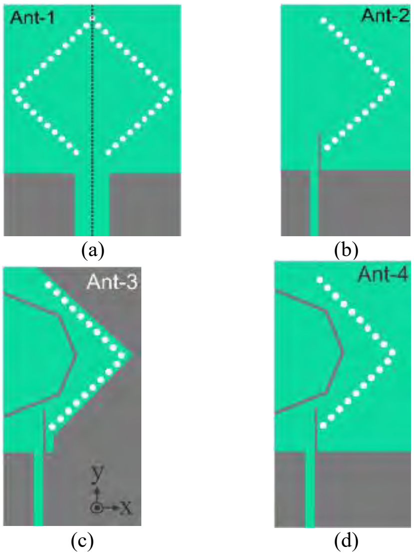

Fig. 1. Evolution of HMSIW antenna (a) basic cavity antenna Ant-1, (b) HMSIW no slot Ant-2, (c) HMSIW with half-octagonal ring slot and without outter Ant-3, (d) HMSIW with half-octagonal ring slot and using outter Ant-4.

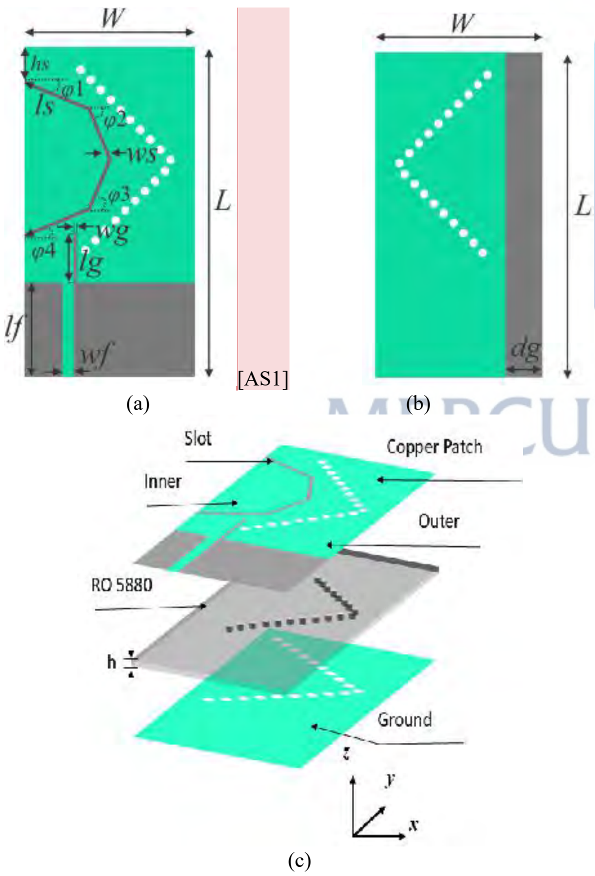

Fig. 2. The design of Ant-4's Half-Mode Substrate-Integrated Waveguide (HMSIW) cavities includes: (a) copper patch geometry, (b) ground plane specifics and (c) HMSIW 3D.

Ant-1 features a basic diamond-shaped within the SIW cavity. The S_{11} parameter indicates an operating bandwidth from 6.62 GHz to 6.96 GHz, with a single resonance. The corresponding impedance bandwidth is 4.9%. The symmetrical slot geometry provides fundamental radiation characteristics but limits bandwidth and gain performance due to constrained excitation of resonant modes.

Ant-2 introduces a HMSIW configuration. This modification alters the current distribution within the cavity, improving impedance matching. The S_{11} parameter shows an operating bandwidth from 5.99 GHz to 6.29 GHz, still with a single resonance. The impedance bandwidth is 5%. Although Ant-2 achieves slightly better bandwidth compared to Ant-1, the gain improvement remains moderate.

Ant-3 incorporates significant refinements, including a more complex with half-octagonal ring slot and optimized cavity parameters. The half-octagonal ring slot of Ant-3 is made up of four segments: one low left-slanted, one high left-slanted, one low right-slanted and one high right-slanted. These segments are positioned at $\varphi1 = -22.5°$, $\varphi2 = -67.5°$, $\varphi3 = 22.5°$ and $\varphi4 = 67.5°$, respectively as shown in Fig. 2. The S_{11} parameter indicates an expanded operating bandwidth from 5.62 GHz to 6.66 GHz due to the dual-resonant frequencies formed by the addition of half-octagonal ring slots in the inside cavity. The impedance bandwidth is 16.9%. These improvements enhance impedance bandwidth.

Ant-4 builds upon the design of Ant-3, incorporating further structural optimizations to the slot and the lower outer cavity as shown in Fig. 2. Specifically, Ant-4 employs a half-octagonal ring slot that acts as the radiating slot inside the cavity. The addition of the lower outer cavity enables improved E-field propagation to this region, which contributes to the widening of the impedance bandwidth. This modification allows the TE_{101} and TE_{102} modes to couple more effectively, resulting in a broader frequency response. The S_{11} parameter shows an expanded operating bandwidth from 5.60 GHz to 6.71 GHz, with a dual-resonant characteristic. The corresponding impedance bandwidth is 18%. Despite these improvements, the maximum gain for Ant-4 remains 2.73 dB over the frequency range of 5 GHz to 7.5 GHz, which is lower than the earlier designs, as shown in Fig. 3 and Fig. 4.

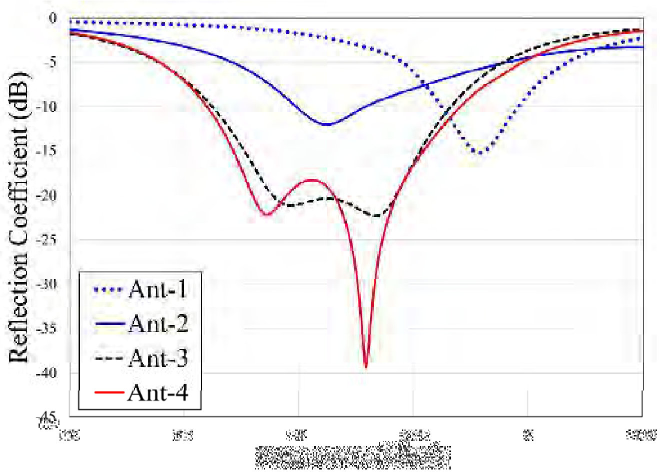

Fig. 3. Simulation of the reflection coefficient for the antenna development in HMSIW cavities.

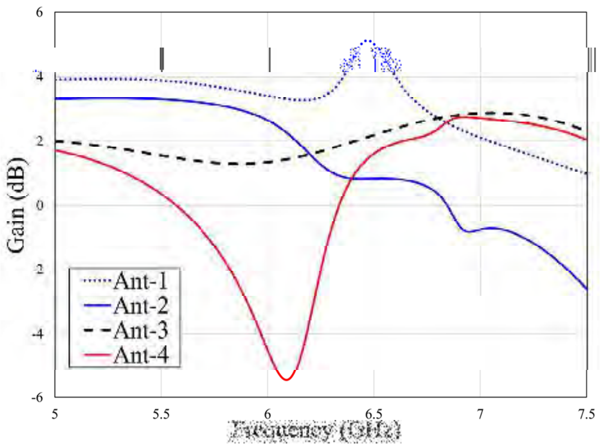

Fig. 4. Simulation of gain.

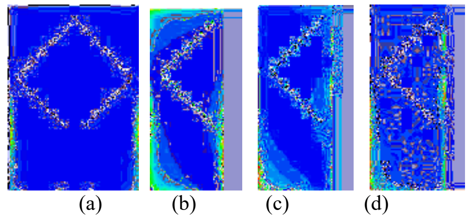

Fig. 5. EFD at center frequency on phase 0° (a) Ant-1 at 6.79 GHz, (b) Ant-2 at 6.35GHz, (c) Ant-3 at 5.96 GHz, (d) Ant-4 at 5.86 GHz.

III. Method and Parametric Study

A. Analysis of Electric Field Distribution

A study of the Electric Field Distribution (EFD) was conducted to examine how TE modes interact and radiate into free space. Fig. 5 displays the EFD for Ant-1 at 6.79 GHz, Ant-2 at 6.35GHz, Ant-3 at 5.96 GHz and Ant-4 at 5.86 GHz. The EFD for Antennas remained steady at 100 V/cm for one period of phase 0°. Observation of the simulated EFD at Ant-1 in Fig. 6 with phases of 0°, 45°, 90° and 180°, there are different electrical distribution patterns observed at a frequency of 6.79 GHz and the vector directions are also different when observed with an internal phase of 45°. There is no electric field propagating on the inside of the antenna, instead the electric field propagates mostly on the lower outer cavity and feeding of the antenna.

For Ant-2 as shown at Fig. 7, the simulated EFD at a frequency of 6.35 GHz reveals a similar pattern to Ant-1. The electric field distribution is observed primarily in the outer-bottom region and the feeding area, with little to no propagation inside the cavity. The vector directions change notably at a phase of 45°, highlighting asymmetric field distribution due to the modified HMSIW. The lack of significant electric field interaction within the cavity limits the excitation of higher-order modes, resulting in a single-resonant behavior and a relatively narrow impedance bandwidth. However, the asymmetry improves impedance matching compared to Ant-1.

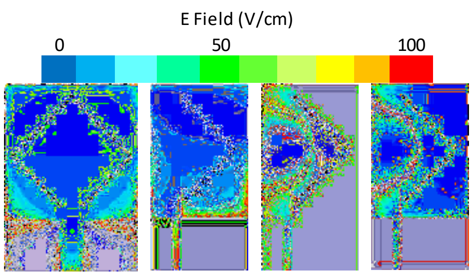

In Ant-3, as shown in Fig. 8, the simulated EFD at a frequency of 5.96 GHz shows improved electric field interaction within the structure. The addition of the half-octagonal slot enhances E-field propagation along the slot side inside the antenna cavity, allowing better coupling between the slot and the cavity. This modification introduces dual-resonant behavior due to the interaction between the TE_{101} and TE_{102} modes, which helps broaden the impedance bandwidth.

The electric field propagates partially into the inner cavity and is also distributed in the half-octagonal slot area and the feeding area. The different patterns observed across phases (0°, 45°, 90°, and 180°) further confirm the presence of this dual-resonant behavior. However, despite the broader impedance bandwidth achieved, the field distribution within the cavity remains limited, which impacts the overall gain performance.

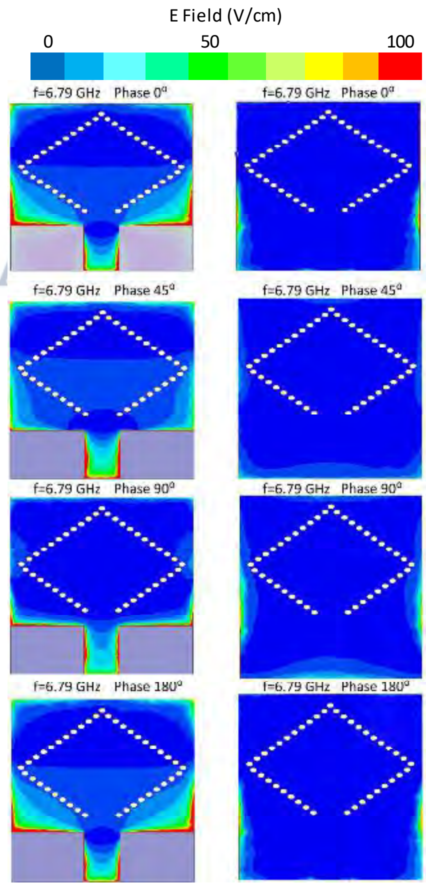

Fig. 6. EFD on Ant-1 at frequency 6.79 GHz.

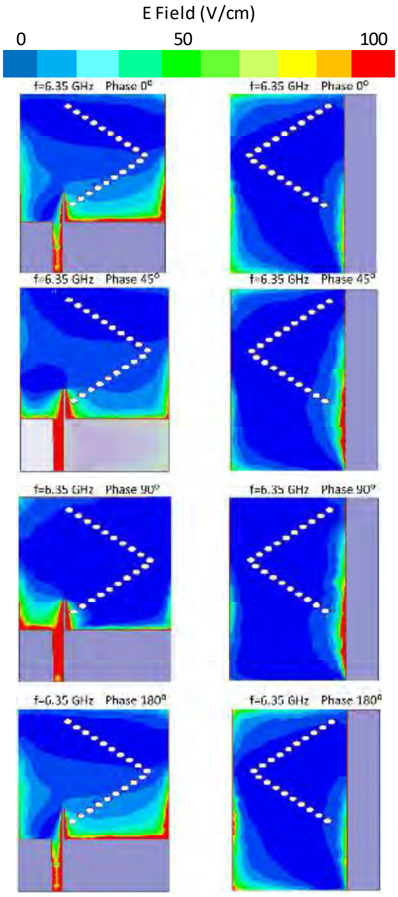

Fig. 7. EFD on Ant-2 at frequency 6.35 GHz.

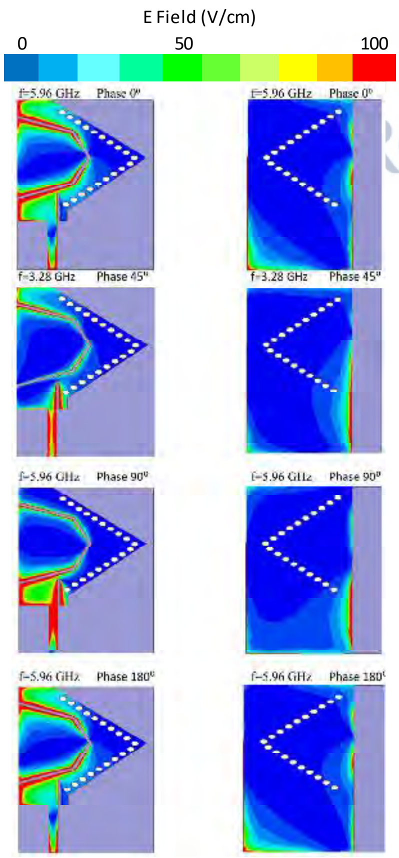

Fig. 8. EFD on Ant-3 at frequency 5.96 GHz.

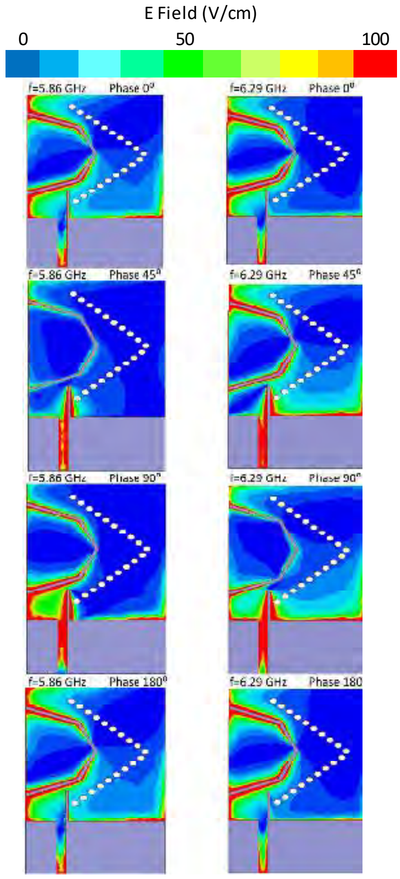

(a) (b)

Fig. 9. EFD on Ant-4 (a) at 5.86 GHz, (b) at 6.29 GHz.

In Ant-4, as shown in Fig. 9, the simulated Electric Field Distribution (EFD) at frequencies of 5.86 GHz and 6.29 GHz exhibits significant improvements in electric field interaction compared to previous designs. The electric field is strongly concentrated in the feeding area, the half-octagonal slot, and the lower outer cavity, which facilitates more effective E-field propagation. This modification results in dual resonance formed by the TE_{101} and TE_{102} modes, contributing to a larger impedance bandwidth than observed in Ant-3. The inner cavity analysis reveals that the first resonant frequency at 5.86 GHz is predominantly characterized by a strong TE_{101} mode and a weak TE_{102} mode, while the second resonant frequency at 6.29 GHz exhibits a strong TE_{102} mode and a weak TE_{101} mode.

In the lower outer cavity, for both frequencies at 5.86 GHz and 6.29 GHz, there is only a single resonance of the TE_{101} mode, consistent with the results of Ant-1 at FMSIW, which also exhibits a single resonance behavior. The distinct patterns observed across phases (0°, 45°, 90°, and 180°) further confirm the presence of this dual-resonant behavior. The enhanced electric field distribution across the lower outer cavity, feeding area, and half-octagonal slot supports a broader impedance bandwidth and improved radiation efficiency. However, the gain performance remains moderate due to the spread of radiation over multiple modes, which reduces the directivity.

B. Parameters Study Bandwidth Enhancement

A parametric study was conducted to analyze the effects of key design parameters on the impedance bandwidth and reflection coefficient (S_{11}) of Ant-4. Three parameters were studied: slot length (*Ls*), slot thickness (*Ws*), and slot position (*Hs*). Each parameter was varied to determine the optimal configuration for the broadest impedance bandwidth.

For the *Ls*, as shown in Fig. 10, values of 17.5 mm, 21.9 mm, 26.15 mm, and 28.0 mm were simulated. The results showed that a slot length of 26.15 mm provided the optimal performance, offering a frequency range of 5.60 GHz to 6.71 GHz, resulting in a bandwidth of 1.11 GHz. For shorter slot lengths of 17.5 mm and 21.9 mm, the first frequency resonance shifts toward higher frequencies, and only a single resonance is observed, leading to narrower bandwidths. In contrast, for slot lengths of 26.15 mm and 28.0 mm, the antenna exhibits dual-resonant behavior due to the merging of the TE_{101} and TE_{102} modes. However, increasing the slot length to 28.0 mm reduces the bandwidth significantly to 0.98 GHz, indicating detuning and less effective coupling.

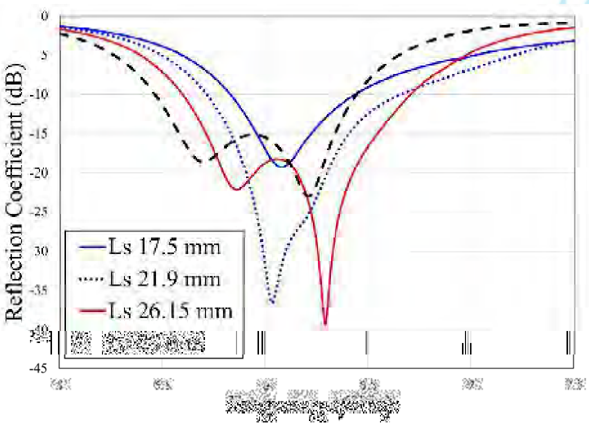

Fig. 10. Simulation of the reflection coefficient for the *Ls* parameter, defined as the length of a half-octagonal ring slot.

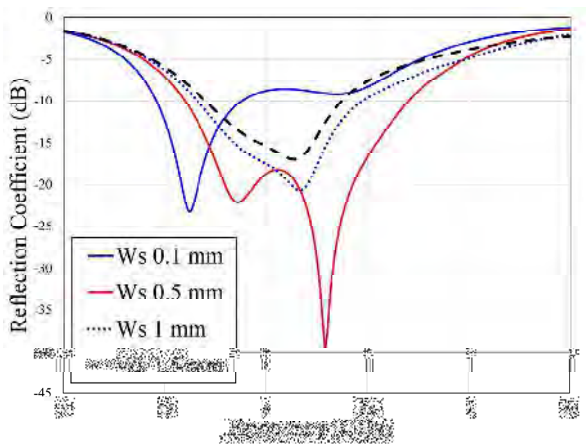

Fig. 11. Simulation of the reflection coefficient for the *Ws* parameter, characterized as the thickness of a half-octagonal ring slot.

The study of the *Ws* as shown at Fig. 11 examined values of 0.1 mm, 0.5 mm, 1.0 mm, and 1.5 mm. The simulations revealed that a slot thickness of 0.5 mm produced the broadest bandwidth, covering the frequency range of 5.60 GHz to 6.71 GHz with a bandwidth of 1.11 GHz. Reducing the thickness to 0.1 mm slightly improved the lower frequency range but showed poorer impedance matching. On the other hand, increasing the thickness to 1.0 mm and 1.5 mm reduced the bandwidth to 0.87 GHz and 0.67 GHz, respectively, indicating weaker coupling and increased reflection.

The *Hs* as shown at Fig. 12 from the top of the patch side was varied with values of 2.5 mm, 3.45 mm, 3.95 mm, and 4.25 mm. The best performance was achieved with a slot position of 3.45 mm, providing a frequency range of 5.60 GHz to 6.71 GHz and a bandwidth of 1.11 GHz. Moving the slot closer to the top edge with 2.5 mm resulted in a slightly broader frequency range but caused impedance mismatching at the upper frequencies. Increasing the slot position to 3.95 mm and 4.25 mm led to a reduction in bandwidth.

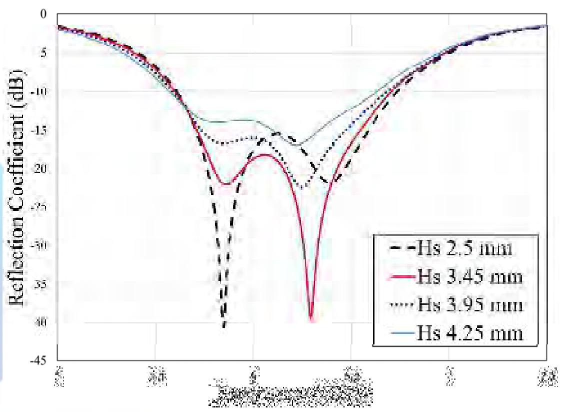

Fig. 12. Simulation of the reflection coefficient for the *Hs* parameter.

C. Antenna Polarization

The polarization characteristics of Ant-4 were evaluated based on the simulation results for the Axial Ratio (AR) across the frequency range of 5 GHz to 7.5 GHz. The axial ratio measures the ratio of the major axis to the minor axis of the electric field vector in the radiated wave and is commonly used to distinguish between linear and circular polarization.

The axial ratio plot for Ant-4 shows a minimum value of 5.6 dB occurring at a frequency of 6.18 GHz. In general, an axial ratio of 3 dB or lower indicates circular polarization, while values significantly higher than 3 dB indicate linear polarization. Since the lowest axial ratio observed for Ant-4 is 5.6 dB, this confirms that the antenna operates with linear polarization throughout its operating bandwidth.

D. Radiation Pattern and Gain Antenna

The radiation pattern of Ant-4 was analyzed at four frequencies of 5.60 GHz, 5.86 GHz, 6.29 GHz and 6.71 GHz as shown at Fig. 13. The simulated results provide insight into the antenna's performance in both the YOZ plane (E-plane) and the XOZ plane (H-plane), focusing on the co-polarization and cross-polarization components. These results highlight the antenna’s ability to radiate energy in multiple directions due to the geometry of the half-octagonal slot etched on the patch side.

At both 5.60 GHz and 5.86 GHz, the co-polarization and cross-polarization radiation patterns exhibit dual-directional behavior, maintaining good polarization purity. In the YOZ plane (E-plane), significant lobes are observed in both forward and backward directions, with strong radiation around ±30° and ±150°. Similarly, in the XOZ plane (H-plane), the co-polarization pattern shows a broader lobe structure peaking near ±90°. Cross-polarization levels remain low at both frequencies, generally below −20 dB, ensuring minimal interference. However, a key difference between the two frequencies is the slight increase in radiation pattern size at 5.86 GHz compared to 5.60 GHz. Despite this difference, the radiation patterns are still similar, validating the antenna's consistent bidirectional radiation capabilities and high polarization purity across the operating bandwidth.

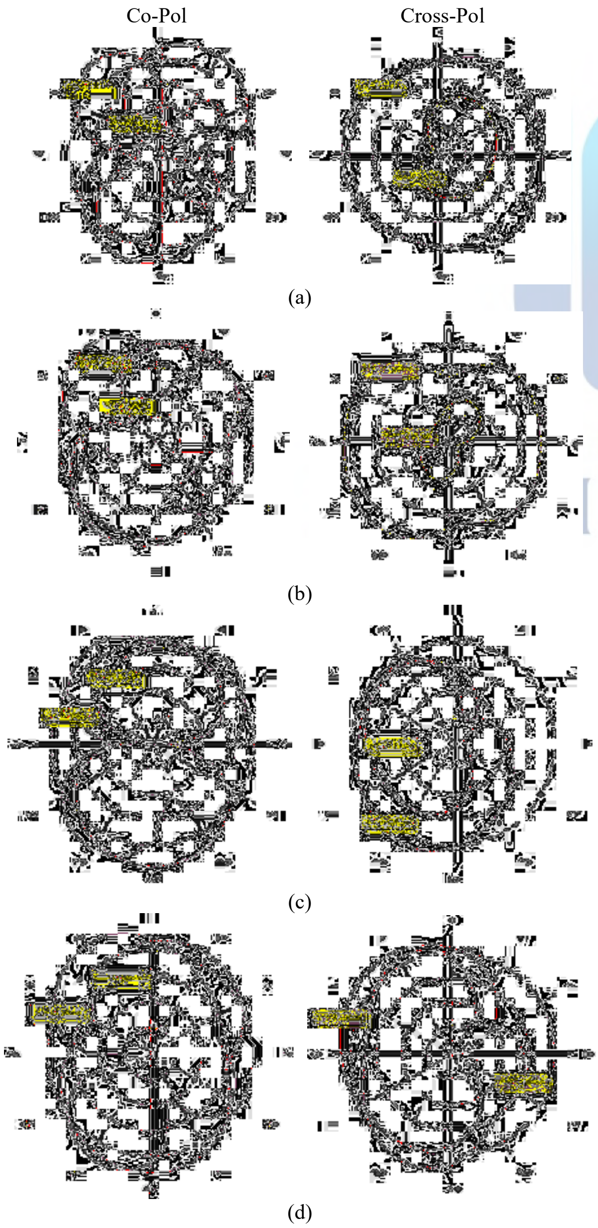

Fig. 13. Simulation of radiation pattern Ant-4 (a) at 5.60 GHz, (b) at 5.86 GHz, (c) at 6.29 GHz and (d) at 6.71 GHz

Building on the consistent performance observed at lower frequencies, the co-polarization patterns at 6.29 GHz and 6.71 GHz continue to exhibit dual-directional lobes in the YOZ plane, with the strongest radiation occurring around ±40° and ±140°, while in the XOZ plane, the radiation remains broad with primary lobes centered near ±90°. Cross-polarization levels at both frequencies are relatively low, generally below −15 dB, ensuring good polarization purity and minimal interference. A notable difference between the two frequencies is the slightly larger radiation pattern at 6.29 GHz compared to 6.71 GHz. Despite this difference, the radiation patterns are still similar, confirming the antenna's stable bidirectional radiation capabilities and effective performance across the higher end of its operating bandwidth.

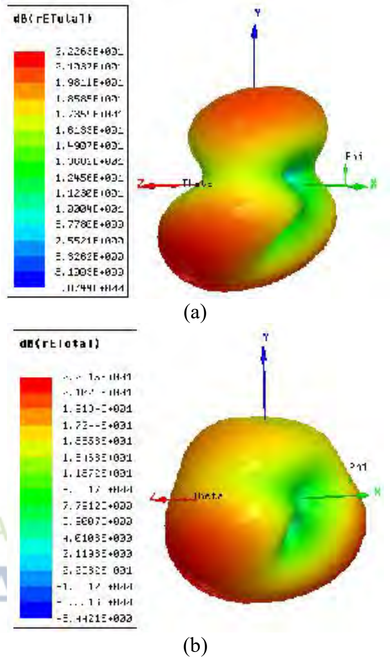

Fig. 14. The 3D polarization for Ant-4 at (a) 5.86 GHz, and (b) 6.29 GHz.

IV. Result and Discussion

Fig. 15 present the fabrication of Ant-4 and the simulation of reflection coefficient (S_{11}). The comparison of the simulated and measured reflection coefficient S_{11} for Ant-4 shows a Fig. 16. The simulated results cover a frequency range of 5.60 GHz to 6.71 GHz, corresponding to an impedance bandwidth of 18%. The measured results from the fabricated prototype indicate an improved impedance bandwidth of 19.4%, covering the frequency range of 5.82 GHz to 7.07 GHz. This slight discrepancy between simulation and measurement can be attributed to fabrication tolerances, material inconsistencies, and connector losses. Variations in the precision of manufacturing processes, such as via-hole placement, slot etching, and alignment, can introduce deviations in the structural geometry of the antenna. These discrepancies may result in shifts in resonant frequencies and slight degradation of impedance matching. Material inconsistencies can arise due to several factors that affect the substrate's properties and overall antenna performance.

Variations in the dielectric properties of the substrate, such as permittivity (ϵ_r) and loss tangent (δ), may occur due to differences in the quality of production batches. Additionally, mechanical damage to the substrate, such as bending or denting, during fabrication or handling, can further contribute to inconsistencies. Imperfections in the SMA connectors or slight misalignments during the experimental setup can introduce additional losses, which may not be captured in simulation. This can contribute to variations in reflection coefficient (S_{11}) and radiation efficiency.

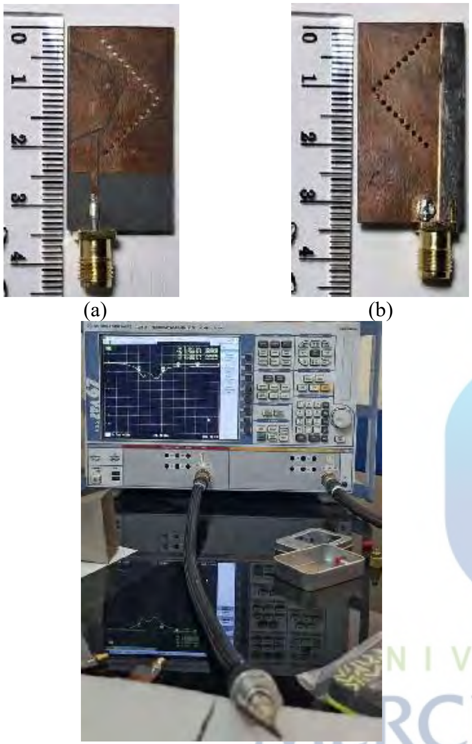
(a) (b) (c)

Fig. 15. (a) The top view and (b) the bottom view of the Ant-4 fabrication (c) Measurement processing of the fabrication Ant-4.

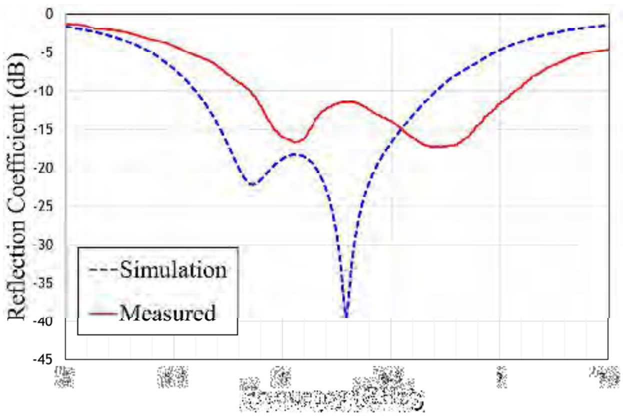

Fig. 16. Simulation and measurement of the reflection coefficient for the proposed antenna.

The proposed Ant-4 achieves a broad impedance bandwidth of 19.4%, covering the frequency range from 5.82 GHz to 7.07 GHz for the fabricated prototype as shown in Fig. 16. While the gain is moderate at 2.73 dBi, the antenna's dual-direction radiation pattern provides versatile coverage suitable for applications like body area networks and wireless communication systems. The simulated results are validated by the measured reflection coefficient and radiation patterns, demonstrating the effectiveness of the design. The radiation pattern measurements for Ant-4 were conducted at frequencies of 6.03 GHz and 6.74 GHz. As shown in the Fig. 17, the measured co-polarization (blue line) and cross-polarization (red line) components reveal that the antenna maintains good polarization purity. At 6.03 GHz, the co-pol pattern shows broad coverage with some directional characteristics, while the cross-pol remains relatively low, indicating minimal polarization leakage. Similarly, at 6.74 GHz, the co-pol pattern exhibits stable performance with a consistent radiation lobe, and the cross-pol remains suppressed. These results confirm that Ant-4 achieves dual-resonant behavior with efficient radiation characteristics.

Compared to previous studies, Ant-4 offers a balanced trade-off between bandwidth, gain, and design complexity. However, the antenna gains of 2.73 dBi is relatively moderate, which may limit its applicability in scenarios requiring higher gain. Future improvements can be achieved by array configurations to increase gain through constructive interference or Frequency Selective Surface (FSS) techniques to enhance radiation efficiency.

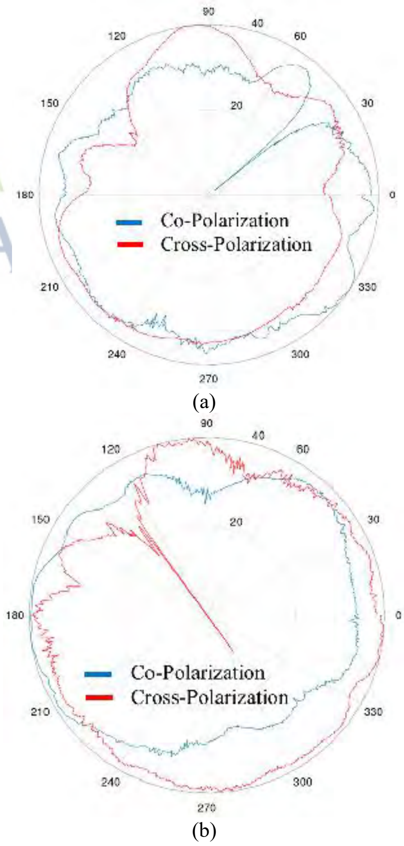

(a)

(b)

Fig. 17. Ant-4 Radiation Pattern measured (a) at 6.03 GHz, (b) at 6.74 GHz

Table III presents a comparative analysis of the proposed antenna's measured performance against previously published research in terms of dimensions, simulated gain, bandwidth, and fractional bandwidth. The proposed antenna exhibits a compact size of 0.73 × 0.52 × 0.01 $(\lambda_0)^3$, which is comparable to other designs while achieving a significantly enhanced bandwidth of 1250 MHz and an FBW of 19.4%, the highest among the listed references. Despite having a lower simulated gain of 2.73 dBi, the superior bandwidth performance suggests improved frequency coverage, making it suitable for broadband applications.

TABLE III. COMPARISON OF THE PROPOSED MEASURED ANTENNA WITH PREVIOUSLY PUBLISHED RESEARCH

Ref	Dimension $(\lambda_0)^3$	Gain Sim. dBi	BW MHz	FBW %
[2]	0.67 × 0.52 × 0.01	5.3	100	1.7
[3]	0.75 × 0.55 × 0.01	4.8	250	4
[6]	0.72 × 0.65 × 0.01	6.2	500	8.5
[9]	0.78 × 0.54 × 0.01	5.5	910	15
[10]	0.80 × 0.55 × 0.01	5.7	700	11.7
[14]	0.73 × 0.60 × 0.01	5.7	1000	16
This Work	0.73 × 0.52 × 0.01	2.73	1250	19.4

V. CONCLUSION

This study presented the design, simulation, fabrication, and measurement of a cavity slot antenna based on SIW technology, referred to as Ant-4. The proposed antenna achieved a dual-resonant frequency range of 5.82 GHz to 7.07 GHz, corresponding to an impedance bandwidth of 19.4%. The two resonant frequencies resulted from the merging of the TE_{101} and TE_{102} modes due to the presence of the optimized half-octagonal slots. The antenna exhibited a dual-directional radiation pattern, radiating energy both forward and backward, making it suitable for applications such as body area networks and wireless communication systems. Despite a moderate gain of 2.73 dBi, the antenna demonstrated reliable performance with good polarization purity and significant bandwidth improvement, future improvements could focus on implementing array configurations to increase gain through constructive interference or utilizing Frequency Selective Surface (FSS) techniques to enhance radiation efficiency.

CONFLICT OF INTEREST

The authors declare no conflict of interest.

AUTHOR CONTRIBUTIONS

Dian Widi Astuti conducted this research; Andri Setyawan performed the simulation and fabrication of the antenna design, Mudrik Alaydrus conducted the antenna measurements, and Yuyu Wahyu analyzed the data; all authors had approved the final version.

ACKNOWLEDGEMENT

The authors would like to thank the Direktorat Jenderal Pendidikan Tinggi, Riset dan Teknologi (Kemenristekdikti), Indonesia, which has funded this research under the Penelitian Tesis Magister scheme with the number 01-1-4/644/SPK/VII/2024.

REFERENCES

[1] Y. Tu *et al.*, "Directivity-enhanced planar slot antenna backed by substrate integrated waveguide cavity," *Microw. Opt. Technol. Lett.*, vol. 65, no. 11, pp. 2919–2925, 2023.
[2] G. Q. Luo, Z. F. Hu, W. J. Li, X. H. Zhang, L. L. Sun, and J. F. Zheng, "Bandwidth-enhanced low-profile cavity-backed slot antenna by using hybrid SIW cavity modes," *IEEE Trans. Antennas Propag.*, vol. 60, no. 4, pp. 1698–1704, 2012.
[3] S. A. Razavi and M. H. Neshati, "Development of a linearly polarized cavity-backed antenna using HMSIW technique," *IEEE* Antennas *Wirel. Propag. Lett.*, vol. 11, no. 3, pp. 1307–1310, 2012.
[4] Q. Wu, S. Member, H. Wang, and C. Yu, "Low-profile circularly polarized cavity-backed," *IEEE Transactions on Antennas and Propagation*, vol. 64, no. 7, pp. 2832–2839, 2016.
[5] S. Yun, D. Y. Kim, and S. Nam, "Bandwidth and efficiency enhancement of cavity-backed slot antenna using a substrate removal," *IEEE Antennas Wirel. Propag. Lett.*, vol. 11, pp. 1458–1461, 2012.
[6] M. Mbaye, J. Hautcoeur, L. Talbi, and K. Hettak, "Bandwidth broadening of dual-slot antenna using Substrate Integrated Waveguide (SIW)," *IEEE Antennas Wirel. Propag. Lett.*, vol. 12, pp. 1169–1171, 2013.
[7] Y. Tao and Z. X. Shen, "Broadband substrate integrated waveguide orthomode transducers," *J. Electromagn. Waves Appl.*, vol. 23, no. 16, pp. 2099–2108, Jan. 2009.
[8] T. Cheng, W. Jiang, S. Gong, and Y. Yu, "Broadband SIW cavity-backed modified dumbbell-shaped slot antenna," *IEEE Antennas Wirel. Propag. Lett.*, vol. 18, no. 5, pp. 936–940, 2019.
[9] H. Dashti and M. H. Neshati, "Development of low-profile patch and semi-circular SIW cavity hybrid antennas," *IEEE Trans. Antennas Propag.*, vol. 62, no. 9, pp. 4481–4488, 2014.
[10] S. Yun, D. Y. Kim, and S. Nam, "Bandwidth enhancement of cavity-backed slot antenna using a Via-hole above the slot," *IEEE Antennas Wirel. Propag. Lett.*, vol. 11, pp. 1092–1095, 2012.
[11] Y. Shi, J. Liu, Y. Long, and S. Member, "Wideband triple- and quad-resonance substrate integrated waveguide cavity-backed slot," *IEEE Transactions on Antennas and Propagation*, vol. 65, no. 11, pp. 5768–5775, 2017.
[12] Q. Wu, J. Yin, C. Yu, H. Wang, and W. Hong, "Broadband planar SIW cavity-backed slot antennas aided by unbalanced shorting vias," *IEEE Antennas Wirel. Propag. Lett.*, vol. 18, no. 2, pp. 363–367, 2019, doi: 10.1109/LAWP.2019.2891108.
[13] L. Xiang, Y. Zhang, Y. Yu, and W. Hong, "Characterization and design of wideband penta-and hepta-resonance SIW elliptical cavity-backed slot antennas," *IEEE Access*, vol. 8, pp. 111987–111994, 2020.
[14] D. W. Astuti, Y. Wahyu, F. Y. Zulkifli, and E. T. Rahardjo, "Hybrid HMSIW cavities antenna with a half-pentagon ring slot for bandwidth enhancement," *IEEE Access*, vol. 11, pp. 18417–18426, 2023.
[15] R. S. Chaturvedi D, Kumar, "Wideband HMSIW-based slotted antenna for wireless fidelity application," *IET Microwaves, Antennas and Propagation*, vol. 13, no. 2, pp. 258–262, 2018.
[16] D. W. Astuti, M. Asvial, F. Y. Zulkifli, and E. T. Rahardjo, "Bandwidth enhancement on half-mode substrate integrated waveguide antenna using cavity-backed triangular slot," *Int. J. Antennas Propag.*, vol. 69, no. 3, 2023.
[17] S. K. K. Dash, Q. S. Cheng, R. K. Barik, F. Jiang, N. C. Pradhan, and K. S. Subramanian, "A compact SIW cavity-backed self-multiplexing antenna for hexa-band operation," *IEEE Trans. Antennas Propag.*, vol. 70, no. 3, pp. 2283–2288, 2022.
[18] D. W. Astuti, R. Muslim, I. Simanjuntak, T. Firmansyah, D. A. Cahyasiwi, and Y. Natali, "Bandwidth enhancement for half mode substrate integrated waveguide antenna using defected ground structures," *Int. J. Electron. Telecommun.*, vol. 69, no. 3, pp. 449–454, 2023.
[19] D. W. Astuti *et al.*, "Bandwidth enhancement for QMSIW antenna by using dual cavity and triangle slot," *Int. J. Electron. Telecommun.*, vol. 70, no. 2, pp. 519–524, 2024.

[20] C. Jin, R. Li, A. Alphones, and X. Bao, "Quarter-mode substrate integrated waveguide and its application to antennas design," *IEEE Trans. Antennas Propag.*, vol. 61, no. 6, pp. 2921–2928, 2013.
[21] J. Qin, X. Fu, M. Sun, Q. Ren, and A. Chen, "Frequency reconfigurable antenna based on substrate integrated waveguide for S-band and C-band applications," *IEEE Access*, vol. 9, pp. 2839–2845, 2021.
[22] J. Zhou and M. Yang, "A Low-Profile Eighth-Mode SIW Antenna With Dual-Sense Circular Polarization, Enhanced Bandwidth and Simple Structure," *IEEE Access*, vol. 9, pp. 144375–144384, 2021.
[23] D. W. Astuti, M. Muslim, U. Umaisaroh, H. A. Majid, S. Alam, and Y. Rahayu, "Broadband HMSIW antenna using a semi hexagonal ring slot for X-band application," *Sinergi (Indonesia)*, vol. 29, no. 1, pp. 73–82, 2025.
[24] D. W. Astuti, H. A. Majid, S. Alam, and A. Setyawan, "A broadband half-mode substrate integrated waveguide," *Journal of Electromagnetic Engineering and Science*, vol. 152, no. January, pp. 55–66, 2025.

Progress In Electromagnetics Research C, Vol. 156, 67–77, 2025

(Received 13 March 2025, Accepted 14 May 2025, Scheduled 26 May 2025)

Half-Mode Substrate Integrated Waveguide Cavity Slot Antenna with Half-Octagonal Ring Slot at S-Band Frequency

Andri Setyawan[1], Dian Widi Astuti[1,*], Mudrik Alaydrus[1], Yuyu Wahyu[2], and Norbahiah Misran[3]

[1]Department of Engineering, Universitas Mercu Buana, Jakarta 11650, Indonesia
[2]Research Centre for Electronics and Telecommunications, Indonesian Institute of Sciences, Bandung 40135, Indonesia
[3]Department of Electrical, Electronic & System Engineering, Faculty of Engineering and Built Environment
Universiti Kebangsaan Malaysia, UKM Bangi, Selangor 43600, Malaysia

ABSTRACT: This paper presents a design of a half-mode substrate integrated waveguide (HMSIW) antenna for S-band frequencies using half-octagonal ring slots to achieve significant bandwidth enhancement. The proposed structure integrates a half-octagonal ring slot within the HMSIW cavity to enhance impedance bandwidth by exciting dual resonant modes — TE_{101} and TE_{102}. The antenna achieves a measured fractional bandwidth (FBW) of 5.6%, corresponding to an operational range of 3.15 to 3.33 GHz, and a simulated FBW of 5.2% from 3.17 to 3.40 GHz. Compared to conventional cavity-backed SIW antennas, this configuration offers a 50% size reduction while maintaining stable gain between 3.1 dBi and 5.6 dBi and exhibiting a directional linear radiation pattern in the horizontal plane. The integration of dual-resonance excitation within a single compact HMSIW cavity represents a significant advancement in bandwidth enhancement for planar antennas. This design offers a feasible and efficient solution for modern wireless applications requiring miniaturized and compact size in S-band frequencies.

1. INTRODUCTION

Substrate integrated waveguide (SIW) antennas are planar antennas that utilize integrated dielectric and metallic via structures within standard printed circuit board (PCB) substrates to emulate waveguide characteristics and support guided electromagnetic wave propagation. SIW antennas offer advantages such as low cost, ease of fabrication, and compatibility with microwave planar circuits [1–3]. However, conventional SIW antennas often suffer from narrow impedance bandwidths, typically below 2%, which restricts their application in broadband systems [1]. To overcome this, several techniques have been developed, including radiator slot modifications to excite hybrid modes within the SIW cavity. For instance, dual-hybrid mode excitation has improved the FBW from 1.4% to 6.3%, along with moderate gain enhancement to 6.0 dBi [4]. Substrate slot removal has also been employed to reduce slot capacitance and widen bandwidth. This method yields a 24% improvement in FBW and a 6.2% increase in antenna efficiency, although it introduces fabrication complexity and retains single-resonant behavior [5]. This approach aims to widen the narrow bandwidth by minimizing the slot capacitance in the traditional cavity back slot (CBS) SIW antenna. Using this technique results in a 24% broader bandwidth and a 6.2% increase in antenna efficiency compared to the conventional CBS SIW design. However, removing the substrate is challenging, and although it broadens the impedance bandwidth, the antenna still resonates at a single frequency, limiting the overall improvement.

Another method for bandwidth enhancement, a design with dual unequal slot radiator modification was performed. The measurements demonstrated 420 MHz impedance bandwidth, which doubles that of the standard dual-slot antenna. Its appealing characteristics such as affordability, small footprint, and flat design facilitate straightforward integration into microwave planar circuits [6]. To achieve miniaturization, half-mode SIW (HMSIW) has been introduced, halving the antenna size but often at the cost of reduced bandwidth performance [7]. Redesigning the radiator using bow-tie slots enabled the generation of closely spaced hybrid modes, achieving a 1.03 GHz and a 3.7 dBi gain at X-band frequencies [8]. Placing the bow-tie-shaped slot at the cavity's top adjusts the loading effect, allowing for the optimization of slot dimensions to generate two closely spaced hybrid modes. These adjustments result in two resonances that significantly enhance bandwidth, contrasting sharply with the 1.7% bandwidth of a conventional slot antenna within an SIW cavity.

Slot geometry has continued to play a central role in bandwidth enhancement. Modified dumbbell slots have generated penta-resonant behavior, producing a wide bandwidth from 18.2 to 23.8 GHz at K-band frequencies [9]. However, this approach typically involves complex slot designs and higher fabrication precision, which may limit its practicality for compact or cost-sensitive applications. SIW CBS antenna design incorporates a hole above the slot to shorten its effective length, thereby creating additional resonances at higher frequencies. This modification enables the antenna to achieve an FBW that is 60% larger than a typical cavity-backed antenna [10]. Several SIW CBS designs have been reported, including a shorting-

* Corresponding author: Dian Widi Astuti (dian.widiastuti@mercubuana.ac.id).

doi:10.2528/PIERC25031301

Published by THE ELECTROMAGNETIC ACADEMY

vias slot achieving quad-resonance at X-band frequencies between 9.36 and 11.26 GHz [11], a cross-shaped design operating from 8.7 to 10.7 GHz [12], and an elliptical CBS covering 8.83–10.99 GHz [13]. These configurations demonstrated significant bandwidth broadening through the use of shorting vias. However, the implementation of such vias presents practical challenges due to the precision required in their placement.

Pin-loaded patches applied at C-band have achieved a 840 MHz bandwidth in the frequency range of 3.62–4.46 GHz, though they suffer from alignment complexity during fabrication [14]. Multi-resonant SIW antennas have also been proposed for hexa-band operation between 5 and 8 GHz, but each sub-band retains a narrow FBW, typically under 2% [15]. The antenna's cavity design incorporates simultaneous port relocation, multilevel patches, and additional vias to mitigate energy leakage between ports, thereby ensuring robust isolation (> 23.42 dB). The antenna produces six working frequencies, but the FBW value is very small at each frequency. The HMSIW CBS antenna with a single resonant frequency [16] has a narrow impedance bandwidth at S-band frequencies with an FBW value of 1.22%.

Several advanced structures, including quad-mode (QM) SIW and eight-mode (EM) SIW, have been implemented to support broader resonance across K-band, C-band, and S-band frequencies, with FBW values ranging from 7.7% to 13.2% [17, 18]. These studies operate in the K-band, C-band, and S-band frequency ranges, achieving FBW values of 7.7%, 13.2%, and 9.1%, respectively. SIWs with modified coupling [19, 20] however still produce relatively small FBWs at 10%, 16.2%, and 4.7%, respectively. The SIW antenna with metamaterial method [21] achieved bandwidth enhancement at C-band frequencies, exhibiting two distinct resonances and covering a frequency span of approximately 1.1 GHz. However, the integration of metamaterials often involves intricate design and fabrication processes. The SIW antenna with rectangular ring slots and long slits were engraved on the top surface of the antenna [22], working in two frequency ranges of S-band and C-band with FBW values of 0.7% and 5.5%, respectively. However, the FBW value obtained was still too small. The bandwidth improvement was achieved through the use of four resonant frequencies [23], which were generated within hybrid HMSIW cavities embedded between the inner and outer substrate layers. These cavities produced closely spaced frequency resonances. This approach is applied specifically to X-band frequencies using a low-profile substrate. Simulation results show an impedance bandwidth of approximately 3.66 GHz, spanning 8.98 to 12.64 GHz, with a peak gain of 7.97 dBi, while measured results indicate a bandwidth around 3.46 GHz, ranging from 9.14 to 12.6 GHz, and a peak gain of 7.62 dBi. Despite its high performance, this method relies on a multilayer structure and precise alignment between layers, which may complicate fabrication and limit scalability for compact or low-cost antenna systems.

Additionally, an HMSIW antenna utilizing a half-rectangular ring slot introduced a triple-resonant mechanism, yielding a measured bandwidth of approximately 3.38 GHz, operating from 7.89 to 11.27 GHz [24]. Similarly, modified I-shaped low-profile HMSIW antennas employing coplanar slot structures have achieved bandwidths greater than 1.85 GHz, covering the range of 8.7 to 10.55 GHz [25]. A wideband hexagonal SIW cavity-backed slot antenna array employing resonant and non-resonant slot combinations achieved an impedance bandwidth of approximately 1.5 GHz, with a measured peak gain of 12 dBi for the array configuration [26]. However, this design involves complex hexagonal geometries and requires precise alignment of multiple elements, which may increase fabrication difficulty and limit suitability for compact.

A half-mode SIW antenna integrated with a U-slot defected ground structure (DGS) achieved bandwidth enhancement of approximately 880 MHz, operating from 5.71 to 6.59 GHz through hybrid resonance of TE_{101} and TE_{102} modes [27]. However, the inclusion of both inner and outer HMSIW cavities, along with the DGS, increases design complexity and sensitivity to fabrication accuracy, which may limit its scalability for compact implementations. A broadband HMSIW antenna design employing a half-octagonal ring slot and outer cavity achieved a measured bandwidth of 1.25 GHz, covering 5.82–7.07 GHz, with a dual-resonant response formed by the merging of TE_{101} and TE_{102} modes [28]. However, the gain remains relatively moderate at 2.73 dBi, which may limit the antenna's applicability in scenarios requiring higher directivity or long-range communication. In this study, a novel approach is introduced using an inner half-mode SIW cavity featuring a half-octagonal ring slot to generate dual-resonant modes (TE_{101} and TE_{102}). These closely spaced resonances significantly enhance the impedance bandwidth. This design achieves a measured FBW of 5.6% in the S-band, with a 50% reduction in antenna size compared to conventional SIW configurations. The major contributions of this work are:

1. A new dual-resonant frequency excitation technique within an HMSIW cavity using a half-octagonal ring slot.
2. The impedance bandwidth improved to 5.6%, covering the frequency range of 3.15 to 3.33 GHz.
3. Maintenance of compact planar structure while preserving gain performance.
4. A significant miniaturization of 50% compared to traditional SIW designs.

2. ANTENNA DESIGN AND MATERIALS

The proposed antenna design, designated as Ant-C as shown in Fig. 1, employs an HMSIW configuration featuring an inner cavity embedded with a half-octagonal ring slot. The antenna is fabricated using a Rogers RT/Duroid 5880 substrate, characterized by a dielectric constant (ε_r) of 2.2, a loss tangent (δ) of 0.0009, and a substrate thickness of 1.575 mm. This configuration achieves a 50% size reduction compared to traditional full-mode SIW (FMSIW) structures while retaining essential wave-guiding properties. Simulations and design optimization were performed using ANSYS HFSS, and mode frequency predictions were based on classical SIW cavity theory [29, 30].

$$f_{mnp}^{SIW} = \frac{1}{2\pi\sqrt{\mu\varepsilon}}\sqrt{\left(\frac{m\pi}{L_{eff}^{SIW}}\right)^2 + \left(\frac{n\pi}{h}\right)^2 + \left(\frac{p\pi}{W_{eff}^{SIW}}\right)^2} \quad (1)$$

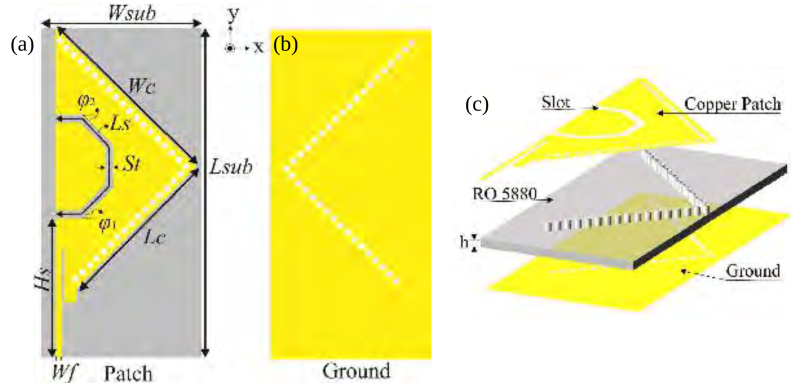

FIGURE 1. The design of Ant-C's HMSIW cavities include: (a) copper patch geometry, (b) ground plane specifics and (c) HMSIW 3D.

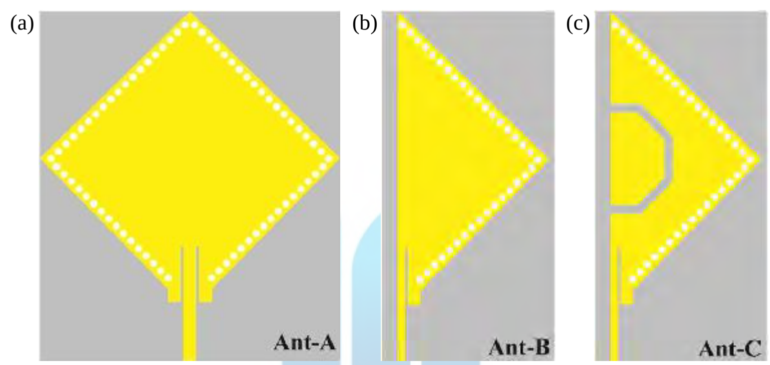

FIGURE 2. Evolution of HMSIW antenna, (a) basic cavity antenna with inner Ant-A, (b) HMSIW no slot Ant-B, (c) HMSIW with half-octagonal ring slot Ant-C.

where $m = 1, 2, ...,$ $n = 1, 2,$ $p = 1, 2, ...$ and $\mu = \mu_0 \cdot \mu_r$, $\varepsilon = \varepsilon_0 \cdot \varepsilon_r$ are the permeability and permittivity of the substrate, respectively. The thickness of the SIW resonator is h. The equivalent length and width (L_{eff}^{SIW} and W_{eff}^{SIW}) are as follows:

$$\begin{cases} L_{\mathit{eff}}^{SIW} = L_c - 1.08\,\frac{D_1^2}{V_3} + 0.1\,\frac{D_1^2}{L_c} \\ W_{\mathit{eff}}^{SIW} = W_c - 1.08\,\frac{D_1^2}{V_3} + 0.1\,\frac{D_1^2}{W_c} \end{cases} \tag{2}$$

$$\lambda_o = \frac{c}{f_c\sqrt{\varepsilon_r}} \tag{3}$$

The dimensions and specifications for Ant-C are presented in Table 1. The structure consists of a rectangular inner cavity modified with a half-octagonal ring slot etched into the top copper layer. This ring is composed of five segments: two horizontal, one vertical, and two diagonally slanted segments positioned at angles $\varphi_1 = -45°$ and $\varphi_2 = 45°$, respectively.

TABLE 1. Dimension of Ant-C (unit in millimeters).

Parameter	W_{sub}	L_{sub}	W_c	L_c	D_1
Value	61	125	53.5	53.5	2.5
Parameter	L_s	S_t	H_s	W_f	V_3
Value	64.2	3	52.94	2.425	3.75

The total slot length is approximately equal to the guided wavelength at the TE_{102} mode of the inner cavity. The slot excites dual resonant frequencies TE_{101} and TE_{102} allowing the antenna to achieve wider impedance bandwidth. The equivalent length and width of the resonator cavity are derived using classical waveguide theory, as shown in Equations (1)–(3). The antenna geometry is shown in Fig. 1, including the top copper patch, ground plane, and a 3D view of the HMSIW structure. The cavity dimensions were optimized to support operation in the S-band range, and the excitation of TE_{101} and TE_{102} modes is confirmed through simulation. The inner cavity is simultaneously fed with 50-ohm matched lines using quarter-wavelength transformers.

The antenna evolution is illustrated in Fig. 2. Ant-A represents the baseline FMSIW cavity design; Ant-B is the 50% miniaturized HMSIW structure without a slot; and Ant-C incorporates a half-octagonal ring slot. The slot perturbation in Ant-C leads to dual-mode excitation, resulting in a wider impedance bandwidth and more stable gain.

The TE modes of the FMSIW were analysed as illustrated in Fig. 3. The anticipated resonant frequencies corresponding to the TE_{101}, TE_{102}, TE_{202}, and TE_{103} modes occurred at frequencies of 2.08, 3.28, 4.17, and 4.67 GHz, respectively. These simulated results were consistent with the calculations shown in Table 2 [30]. TE mode simulations for the inner FMSIW cavity are summarized in Table 2 and visualized in Fig. 3. The narrowband nature and poor reflection coefficient of Ant-A are evident

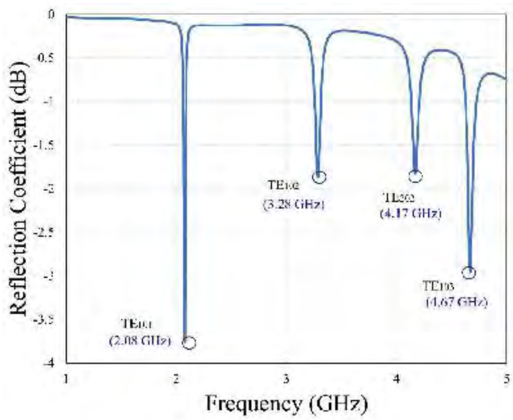

FIGURE 3. Simulation of the reflection coefficient for Ant-A's FMSIW.

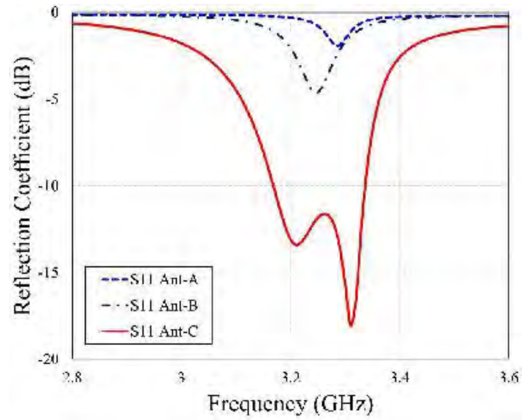

FIGURE 4. Simulated reflection coefficients for the progressive development of HMSIW cavity antennas.

TABLE 2. The calculated sequence of TE modes for the inner FMSIW cavities.

m\p	1	2	3	4	5
1	1.99	3.15	4.45	5.81	7.18
2		3.98	5.08	6.30	7.58
3				7.04	8.21
4				7.97	9.02
5					9.96

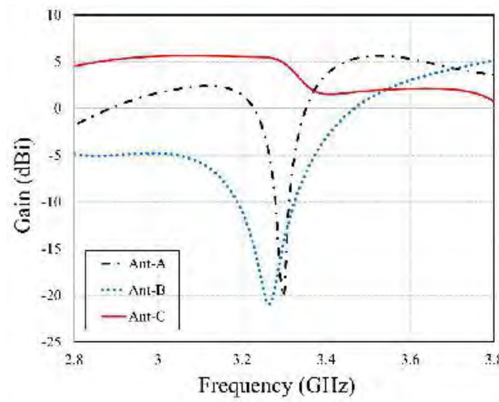

FIGURE 5. Peak realized gain of HMSIW.

in Fig. 3. Fig. 4 presents the reflection coefficient improvements across Ant-B and Ant-C. The reflection coefficient evolution in Fig. 4 confirms that bandwidth broadening is achieved only in Ant-C.

The surface current distributions also affirm strong excitation of the slot at resonant frequencies. The implementation of the half-octagonal slot thus enables the merging of multiple TE modes, significantly improving bandwidth without sacrificing compactness.

Figure 5 demonstrates that Ant-C exhibits a consistently high and flatter realized gain profile, maintaining values above 5 dBi across the operational bandwidth of 3.17–3.34 GHz, with a peak gain of 5.47 dBi at 3.26 GHz. This enhancement is attributed to the dual-mode excitation of TE_{101} and TE_{102}, facilitated by the incorporation of the half-octagonal ring slot within the HMSIW cavity. Compared to Ant-A and Ant-B, which primarily operate in single-mode resonance, Ant-C achieves superior and more stable gain characteristics, while Ant-B reaches a slightly lower peak of 5.13 dBi at 3.8 GHz. The dual-resonance operation in Ant-C contributes to improved radiation performance and flatter gain response over the desired S-band frequency range.

3. METHODS AND PARAMETRIC STUDY

3.1. Electric Field Mode Analysis

The antenna was modelled based on actual physical parameters and boundary conditions. The simulation domain was configured with a radiation boundary and wave ports for realistic excitation and termination. A high-density mesh refinement was applied around the slot region, feedline, and cavity to improve numerical accuracy during parameter sweeps.

The electric field distribution (EFD) is analysed to examine the interaction of TE modes and their radiation behaviour into free space. Fig. 6 displays the EFD for Ant-A at 2.08 GHz. The EFD for Ant-A remains steady at 150 V/cm across one period for each 45° phase interval. In the observation of the simulated EFD at Ant-A in Fig. 6 there is a different electric distribution pattern from Fig. 7 observed at a frequency of 3.28 GHz, and the vector direction is also different when being observed with an internal phase of 45°.

Ant-C can produce dual resonant frequencies, resulting from combinations of the TE_{101} and TE_{102} modes. In Ant-C, the EFD is observed at 3.21 GHz, 3.26 GHz, and 3.31 GHz with phases 0°, 90°, 180°, and 270° as shown in Fig. 8. In Ant-C, the EFD is recorded at 150 V/cm per period, with measurements taken at 90° phase intervals. The EFD on Ant-C at 3.21 GHz arises from the interaction of the strong TE_{101} mode and weak TE_{102} mode combination. Fig. 8(a) illustrates the initial EFD at 3.21 GHz.

The highest electric field intensity within the inner HMSIW was observed along the horizontal, vertical, and both right and left slanted segments of the half-octagonal ring slot. Within the HMSIW structure, the field distribution arises from the combination of a dominant TE_{101} mode and a weaker TE_{102} mode occurring in-phase.

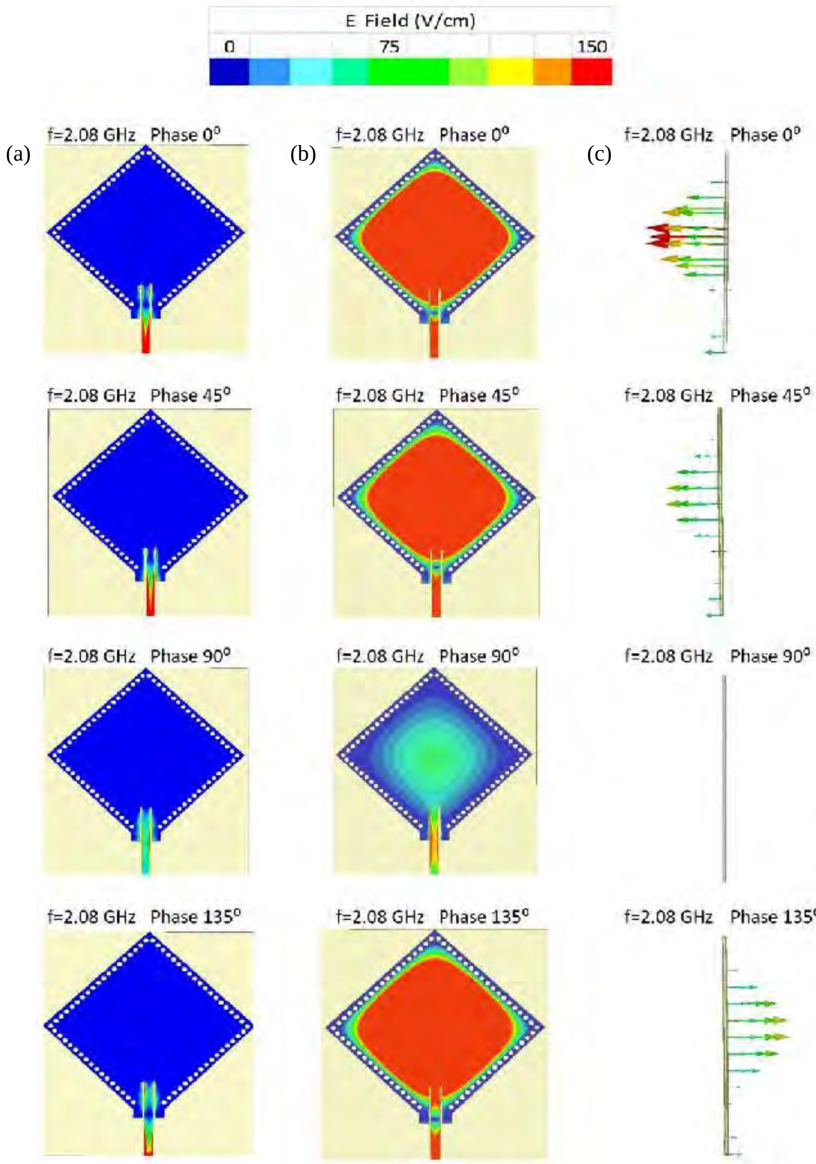

FIGURE 6. EFD of Ant-A at 2.08 GHz on phase 0°, 45°, 90° and 135°, (a) front patch, (b) back patch, (c) Vector E.

The second set of dual resonant frequencies appears at 3.31 GHz, as illustrated in Fig. 8(c). The highest EFD was found in the upper and lower sections of the half-octagonal ring slots within the inner HMSIW. At 3.31 GHz, the field distribution is produced by the interaction of a weaker TE_{101} mode and a stronger TE_{102} mode occurring out of phase. Additionally, significant distribution was observed in the feeding insert area of the HMSIW.

3.2. Parametric Analysis of Bandwidth enhancement

To understand the effect of the radiating slot's physical length (L_s) on bandwidth performance, a systematic parametric sweep was conducted while keeping other structural parameters fixed. The initial slot length was derived from the guided wavelength (λ_g) corresponding to the TE_{102} mode. The analysis indicated that shorter slot lengths weakened field interaction, while longer slots pushed upper-mode resonances outside the operating band. The slot was optimized to simultaneously excite TE_{101} and TE_{102} modes, enabling a broadened bandwidth configuration. The final chosen slot length offered optimal impedance matching and stable resonance behaviour across the S-band.

The slot thickness (S_t) was varied to evaluate its influence on the electromagnetic field behavior within the cavity. A thinner slot restricted field distribution, while excessive thickness resulted in the emergence of undesired parasitic modes. The optimal slot thickness enabled effective field interaction and supported stable dual-resonance operation, all while preserving the antenna's structural simplicity. This configuration proved essential for maintaining consistent performance across the desired frequency range.

Another key variable analysed was the vertical slot position (H_s) relative to the central axis of the HMSIW cavity. Centre-aligned slots supported strong TE_{101} excitation but limited interaction with higher-order modes. Asymmetrical placement

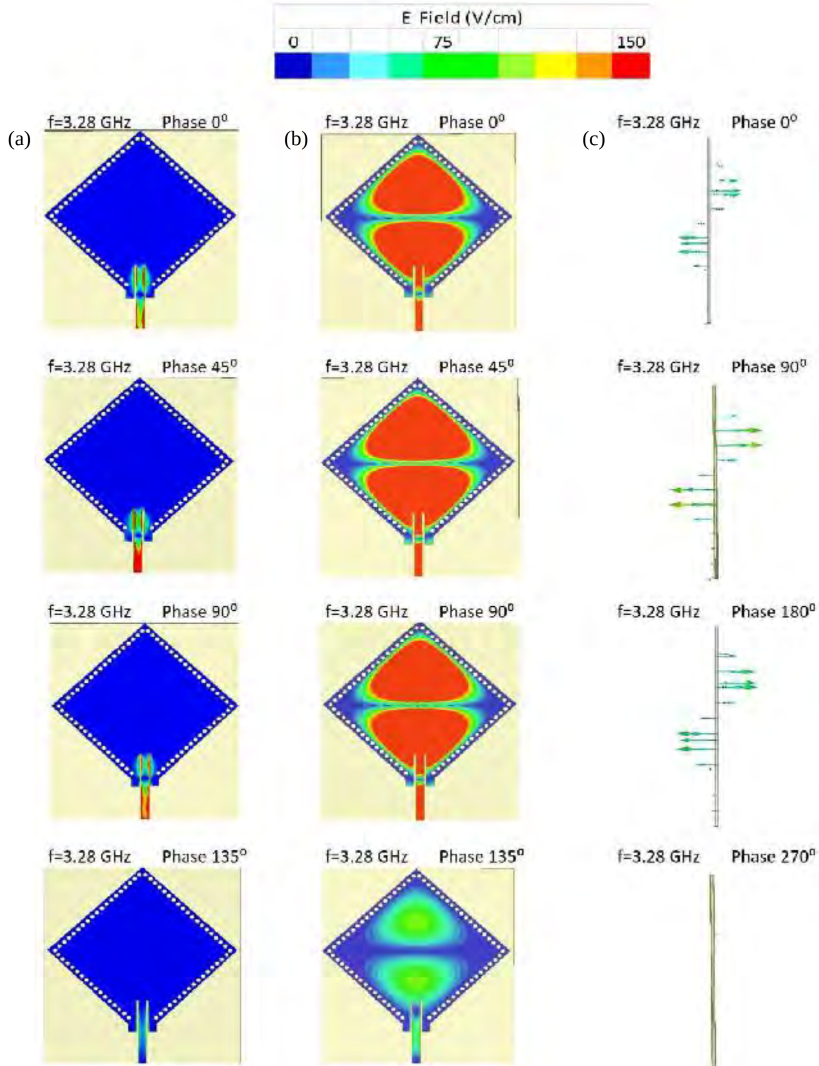

FIGURE 7. EFD of Ant-A at 3.28 GHz on phase 0°, 45°, 90° and 135°, (a) front patch, (b) back patch, (c) Vector E.

toward the top improved TE_{102} mode excitation. A suitable offset was identified that maximized the overlap between the two modes without introducing significant field distortion or degrading the radiation pattern.

4. RESULT AND DISCUSSION

The impact of varying the physical parameters of the radiating slot on the antenna's impedance bandwidth and mode behaviour was investigated using simulation analysis. The key results for slot length, thickness, and vertical position are summarized and discussed below.

The impact of the slot length (L_s) on the antenna's impedance bandwidth was evaluated through simulation, as presented in Fig. 9. The reference slot length was calculated based on the guided wavelength (λ_g) at the TE_{102} mode resonance, determined to be 64.85 mm using Formula (3). At this nominal length, the antenna achieved an FBW of 5.2%. To investigate sensitivity, the slot length was varied as a multiple of λ_g. When $L_s = 0.96\lambda_g$, the antenna exhibited a reduced FBW of 2.6%, with a narrow operational range between 3.08 and 3.16 GHz. Increasing the slot length to $1.03\lambda_g$ resulted in an FBW of 3.7%, extending the frequency range to 3.22–3.34 GHz. However, further extension to $1.09\lambda_g$ failed to maintain adequate impedance matching, as the reflection coefficient did not remain below -10 dB across the band. These results demonstrate that the optimal slot length lies close to the theoretical guided wavelength to enable effective dual-mode excitation and broad bandwidth performance.

The influence of the slot thickness S_t defined as the width of the half-octagonal ring slot was also investigated to determine its effect on bandwidth performance, as illustrated in Fig. 10. The optimal FBW was achieved when $S_t = 3.0$ mm, yielding a 5.2% bandwidth with effective dual-mode excitation. When the slot thickness was increased to 3.4 mm, the FBW slightly decreased to 4.6%, with the operational frequency range extending from 3.19 to 3.34 GHz. Reducing the slot thickness to 2.0 mm resulted in a further decrease in FBW to 2.9%, operating between 3.10 and 3.19 GHz. At the minimum tested thickness of 1.0 mm, the FBW was significantly reduced to 2.3%, with a narrow frequency range from 3.02 to 3.09 GHz. These findings indicate that slot thickness plays a critical role in field

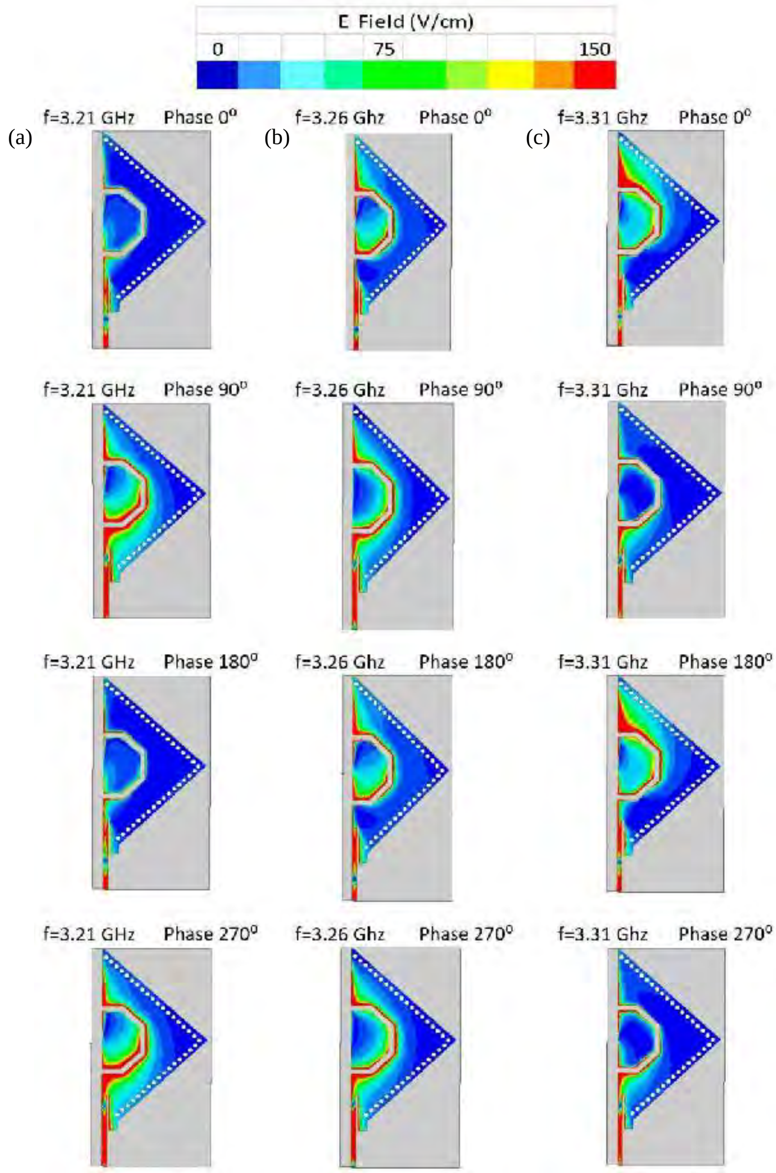

FIGURE 8. EFD of Ant-C at (a) 3.21 GHz, (b) 3.26 GHz, (c) 3.31 GHz on phase 0°, 90°, 180° and 270°.

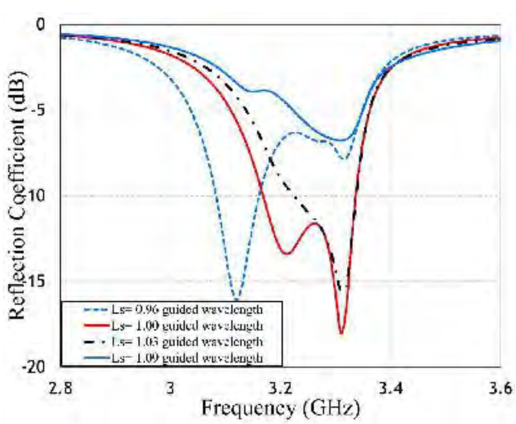

FIGURE 9. Simulated reflection coefficient for the L_s parameter, indicating the length of the half-octagonal ring slot.

coupling efficiency and that 3.0 mm offers an optimal trade-off between bandwidth broadening and mode stability.

The effect of the slot position H_s defined as the vertical distance from the feed point to the centre of the half-octagonal ring slot was analysed to determine its impact on impedance bandwidth. As shown in Fig. 11, the optimal configuration was found when $H_s = 52.94$ mm, which resulted in an FBW of 5.2%, covering the frequency range from 3.17 to 3.34 GHz. When the slot was slightly lowered to $H_s = 52.64$ mm, the FBW decreased to 3.1%, with an operating band from 3.17 to 3.27 GHz. Conversely, increasing the slot position to $H_s = 53.24$ mm further reduced the FBW to 1.2%, spanning 3.32 to 3.36 GHz. At the maximum tested position, $H_s = 53.54$ mm, the reflection coefficient failed to drop below -10 dB, indicating poor impedance matching and ineffective resonance. These results confirm that precise slot positioning is critical for achieving effective dual-mode excitation, and that $H_s =$

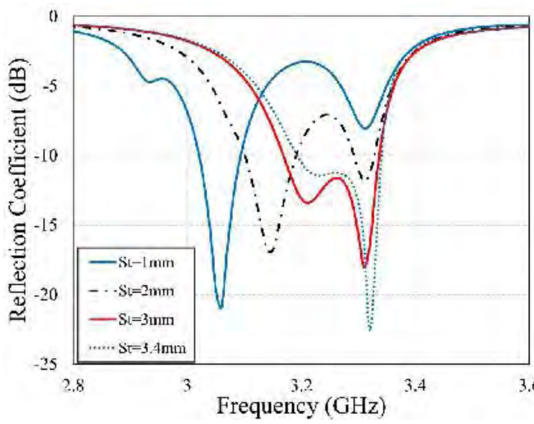

FIGURE 10. Simulated reflection coefficient for the S_t parameter, representing the thickness of the half-octagonal ring slot.

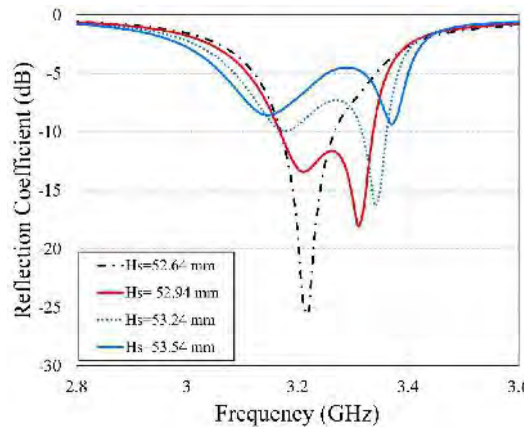

FIGURE 11. Simulated reflection coefficient for the H_s parameter, representing the position of the half-octagonal ring slot.

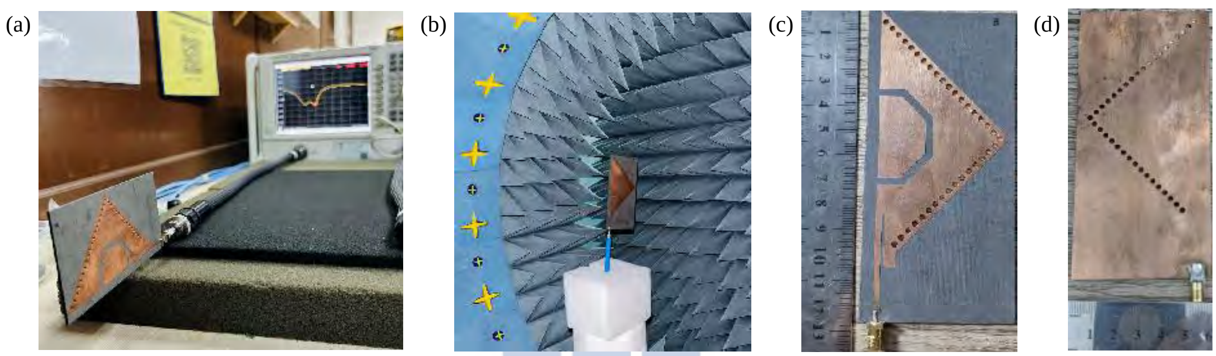

FIGURE 12. Fabricated antenna: (a) S_{11} measurement, (b) radiation pattern measurement, (c) patch view, (d) ground view.

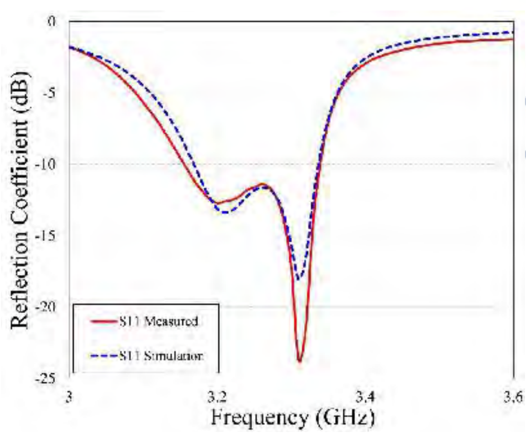

FIGURE 13. Simulation and measured reflection coefficients of the proposed antenna.

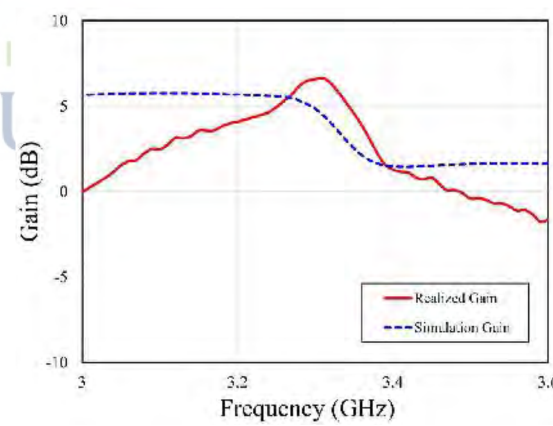

FIGURE 14. Realized and simulated gains of the proposed antenna.

52.94 mm provides the best alignment for broadband performance.

The fabricated antenna, shown in Fig. 12, was produced through a conventional photo etching technique The prototype was tested using a Vector Network Analyzer (VNA) to validate the simulated impedance bandwidth. As shown in Fig. 12(a), the measured reflection coefficient indicates that the antenna achieves a -10 dB impedance bandwidth of 180 MHz, corresponding to a frequency range of 3.15 to 3.33 GHz. This result closely aligns with the simulated bandwidth of 170 MHz, which spans 3.17 to 3.34 GHz. As illustrated in Fig. 13, the measured data exhibit minimal deviation from the simulation results. These minor discrepancies can be attributed to practical fabrication tolerances, variations in the placement of shorting vias, and potential inconsistencies in connector soldering. Despite these factors, the fabricated prototype confirms the antenna's capability to achieve broadband S-band performance with consistent impedance matching characteristics.

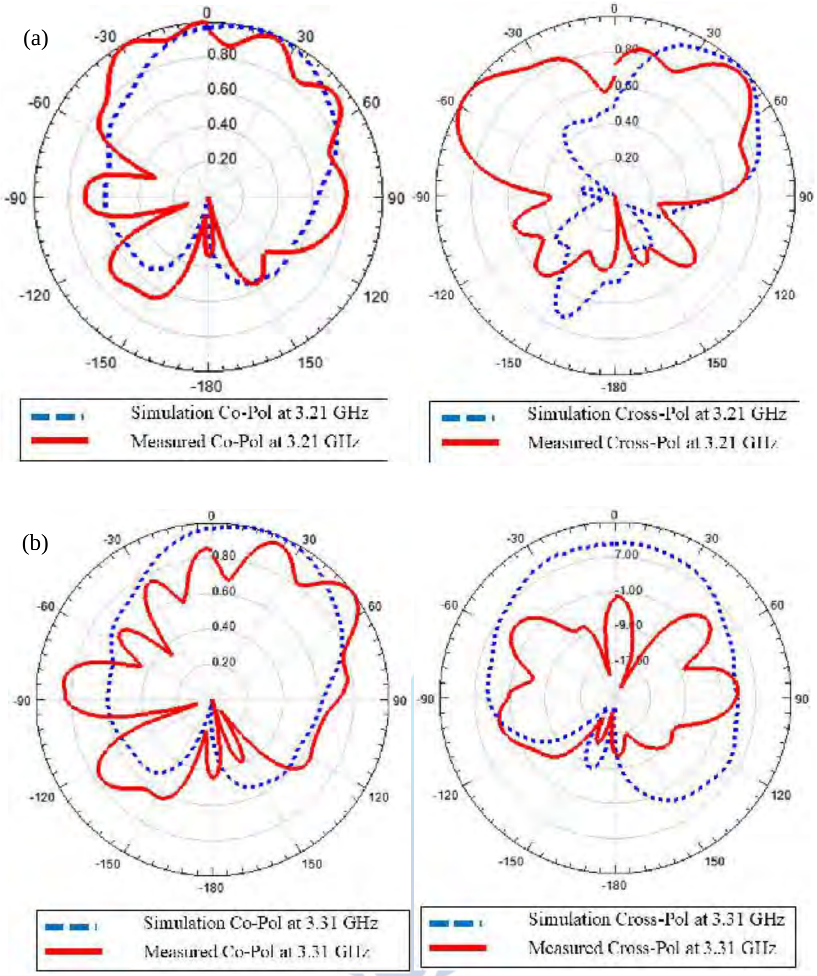

FIGURE 15. Simulation and measured radiation patterns at dual-resonant frequencies, (a) 3.21 GHz and (b) 3.31 GHz.

TABLE 3. Comparison of the proposed measured antenna with previously published research.

Ref.	Dimension (λ_o)	Gain Sim. dBi	F_c GHz	BW MHz	FBW %
[10]	$0.51 \times 0.45 \times 0.01$	5.8	2.45	82	3.3
[16]	$0.22 \times 0.34 \times 0.01$	4.12	2.45	30	1.22
[20]	$0.57 \times 0.54 \times 0.02$	5.74	3.4	160	4.7
[22]	$0.42 \times 0.42 \times 0.01$	2.37	2.41	18	0.75
This Work	$1.31 \times 0.64 \times 0.01$	5.6	3.24	180	5.6

The gain performance of the proposed antenna was analyzed through both simulation and measurement across the frequency range of 3–3.6 GHz, as illustrated in Fig. 14. The simulated gain exhibits a smooth and consistent trend, peaking at approximately 5.75 dBi within the operational band of 3.1–3.2 GHz, confirming the effective excitation of the TE_{101} and TE_{102} modes in the HMSIW cavity. The measured (realized) gain, although showing more fluctuation, gradually increases from negative values at lower frequencies and reaches a peak of approximately 6.63 dBi at 3.31 GHz, before tapering off at higher frequencies. The difference between simulated and measured gains is attributed to practical factors such as fabrication tolerance, connector losses, and measurement environment variations. Nevertheless, the overall consistency in peak gain and frequency behavior between the two datasets affirms the antenna's stable and directional radiation characteristics throughout the S-band frequency range.

Figure 15 presents the normalized radiation pattern of the proposed antenna based on both simulated and measured results at the dual resonant frequencies of 3.21 GHz and 3.31 GHz. The simulation was performed for the principal planes, specifically the E-plane ($\varphi = 0°$) and H-plane ($\varphi = 90°$), which correspond to the antenna's broadside and orthogonal directions, respectively. The results indicate a strong correlation between simulation and measurement, particularly in the co-polarization patterns. Although the two planes exhibit similar directional characteristics, a minor deviation is detected in the main beam direction. This variation is attributed to electromagnetic interactions within the inner HMSIW cavity, specifically influenced by the EFD across the half-octagonal ring slot, as previously illustrated in Fig. 8.

Table 3 presents a comparative evaluation between the proposed antenna and previously reported designs in the literature. The integration of HMSIW cavities with dual-resonant frequencies in the proposed design has effectively enhanced the impedance bandwidth. The measured FBW reaches 5.6%, which exceeds the performance of many conventional SIW cavity-slot antennas operating in the S-band frequency range. While some earlier works achieved broader bandwidths, they typically involvef structurally complex solutions such as stacked substrates, shorting vias, or multilayer configurations. In contrast, the proposed antenna maintains a compact, single-layer structure, offering a favorable balance between electrical performance and fabrication simplicity.

5. CONCLUSION

In this paper, an HMSIW cavity antenna incorporating a half-octagonal ring slot has been designed, simulated, and experimentally validated to enhance impedance bandwidth for S-band applications. The integration of dual-resonant modes, TE_{101} and TE_{102}, within a compact HMSIW structure enabled the antenna to achieve a simulated fractional bandwidth of 5.2% (3.17–3.34 GHz) and a measured FBW of 5.6% (3.15–3.33 GHz), with consistent gain performance ranging from 3.1 dBi to 5.6 dBi and a directional radiation pattern. The proposed design achieves bandwidth enhancement using a single-layer cavity configuration, without requiring complex fabrication techniques such as multilayer stacking or shorting vias. This approach offers a practical and efficient solution for compact wireless systems operating in the S-band. The findings confirm that dual-mode excitation using a half-octagonal ring slot represents a valuable method for bandwidth improvement, with future potential in reconfigurable and multi-band antenna designs.

ACKNOWLEDGEMENT

Thank you to Direktorat Riset, Teknologi, dan Pengabdian Kepada Masyarakat (Kemdiktisaintek), Indonesia, which has funded this research under the Penelitian Tesis Mahasiswa scheme with the number 01-1-4/644/SPK/VII/2024 and Universiti Kebangsaan Malaysia for the supporting the antenna measurement.

REFERENCES

[1] Luo, G. Q., Z. F. Hu, L. X. Dong, and L. L. Sun, "Planar slot antenna backed by substrate integrated waveguide cavity," *IEEE Antennas and Wireless Propagation Letters*, Vol. 7, 236–239, 2008.

[2] Luo, G. Q., T. Y. Wang, and X. H. Zhang, "Review of low profile substrate integrated waveguide cavity backed antennas," *International Journal of Antennas and Propagation*, Vol. 2013, No. 1, 746920, 2013.

[3] Bozzi, M., A. Georgiadis, and K. Wu, "Review of substrate-integrated waveguide circuits and antennas," *IET Microwaves, Antennas & Propagation*, Vol. 5, No. 8, 909–920, Jun. 2011.

[4] Luo, G. Q., Z. F. Hu, W. J. Li, X. H. Zhang, L. L. Sun, and J. F. Zheng, "Bandwidth-enhanced low-profile cavity-backed slot antenna by using hybrid SIW cavity modes," *IEEE Transactions on Antennas and Propagation*, Vol. 60, No. 4, 1698–1704, 2012.

[5] Yun, S., D.-Y. Kim, and S. Nam, "Bandwidth and efficiency enhancement of cavity-backed slot antenna using a substrate removal," *IEEE Antennas and Wireless Propagation Letters*, Vol. 11, 1458–1461, 2012.

[6] Razavi, S. A. and M. H. Neshati, "Development of a linearly polarized cavity-backed antenna using HMSIW technique," *IEEE Antennas and Wireless Propagation Letters*, Vol. 11, 1307–1310, 2012.

[7] Mbaye, M., J. Hautcoeur, L. Talbi, and K. Hettak, "Bandwidth broadening of dual-slot antenna using substrate integrated waveguide (SIW)," *IEEE Antennas and Wireless Propagation Letters*, Vol. 12, 1169–1171, 2013.

[8] Mukherjee, S., A. Biswas, and K. V. Srivastava, "Broadband substrate integrated waveguide cavity-backed bow-tie slot antenna," *IEEE Antennas and Wireless Propagation Letters*, Vol. 13, 1152–1155, 2014.

[9] Cheng, T., W. Jiang, S. Gong, and Y. Yu, "Broadband SIW cavity-backed modified dumbbell-shaped slot antenna," *IEEE Antennas and Wireless Propagation Letters*, Vol. 18, No. 5, 936–940, 2019.

[10] Yun, S., D.-Y. Kim, and S. Nam, "Bandwidth enhancement of cavity-backed slot antenna using a via-hole above the slot," *IEEE Antennas and Wireless Propagation Letters*, Vol. 11, 1092–1095, 2012.

[11] Shi, Y., J. Liu, and Y. Long, "Wideband triple- and quad-resonance substrate integrated waveguide cavity-backed slot antennas with shorting vias," *IEEE Transactions on Antennas and Propagation*, Vol. 65, No. 11, 5768–5775, 2017.

[12] Wu, Q., J. Yin, C. Yu, H. Wang, and W. Hong, "Broadband planar SIW cavity-backed slot antennas aided by unbalanced shorting vias," *IEEE Antennas and Wireless Propagation Letters*, Vol. 18, No. 2, 363–367, 2019.

[13] Xiang, L., Y. Zhang, Y. Yu, and W. Hong, "Characterization and design of wideband penta- and hepta-resonance SIW elliptical cavity-backed slot antennas," *IEEE Access*, Vol. 8, 111 987–111 994, 2020.

[14] Zhang, X., T.-Y. Tan, Q.-S. Wu, L. Zhu, S. Zhong, and T. Yuan, "Pin-loaded patch antenna fed with a dual-mode SIW resonator for bandwidth enhancement and stable high gain," *IEEE Antennas and Wireless Propagation Letters*, Vol. 20, No. 2, 279–283, 2021.

[15] Dash, S. K. K., Q. S. Cheng, R. K. Barik, F. Jiang, N. C. Pradhan, and K. S. Subramanian, "A compact SIW cavity-backed self-multiplexing antenna for hexa-band operation," *IEEE Transactions on Antennas and Propagation*, Vol. 70, No. 3, 2283–2288, 2021.

[16] Astuti, D. W. and E. T. Rahardjo, "Size reduction of cavity backed slot antenna using half mode substrate integrated waveguide structure," in *2018 4th International Conference on Nano Electronics Research and Education (ICNERE)*, 1–4, Hamamatsu, Japan, Nov. 2018.

[17] Wu, Q., H. Wang, C. Yu, and W. Hong, "Low-profile circularly polarized cavity-backed antennas using SIW techniques," *IEEE Transactions on Antennas and Propagation*, Vol. 64, No. 7,

2832–2839, 2016.

[18] Chaturvedi, D., A. Kumar, and S. Raghavan, "Wideband HMSIW-based slotted antenna for wireless fidelity application," *IET Microwaves, Antennas & Propagation*, Vol. 13, No. 2, 258–262, 2019.

[19] Dashti, H. and M. H. Neshati, "Development of low-profile patch and semi-circular SIW cavity hybrid antennas," *IEEE Transactions on Antennas and Propagation*, Vol. 62, No. 9, 4481–4488, 2014.

[20] Zhou, J. and M. Yang, "A low-profile eighth-mode SIW antenna with dual-sense circular polarization, enhanced bandwidth and simple structure," *IEEE Access*, Vol. 9, 144 375–144 384, 2021.

[21] Caytan, O., S. Lemey, S. Agneessens, D. V. Ginste, P. Demeester, C. Loss, R. Salvado, and H. Rogier, "Half-mode substrate-integrated-waveguide cavity-backed slot antenna on cork substrate," *IEEE Antennas and Wireless Propagation Letters*, Vol. 15, 162–165, 2015.

[22] Qin, J., X. Fu, M. Sun, Q. Ren, and A. Chen, "Frequency reconfigurable antenna based on substrate integrated waveguide for S-band and C-band applications," *IEEE Access*, Vol. 9, 2839–2845, 2020.

[23] Astuti, D. W., Y. Wahyu, F. Y. Zulkifli, and E. T. Rahardjo, "Hybrid HMSIW cavities antenna with a half-pentagon ring slot for bandwidth enhancement," *IEEE Access*, Vol. 11, 18 417–18 426, 2023.

[24] Astuti, D. W., H. A. Majid, S. Alam, and A. Setyawan, "A broadband half-mode substrate integrated waveguide cavity antenna with triple-resonances," *Progress In Electromagnetics Research C*, Vol. 152, 55–66, 2025.

[25] Srinivas, L., G. A. Kumar, and G. Ram, "A novel design of modified I-shaped low profile broadband cavity-backed SIW slot antenna," *Journal of Electromagnetic Waves and Applications*, Vol. 38, No. 6, 724–737, 2024.

[26] Astuti, D. W., M. Muslim, U. Umaisaroh, H. A. Majid, S. Alam, and Y. Rahayu, "Broadband HMSIW antenna using a demi hexagonal ring slot for X-band application," *Sinergi (Indonesia)*, Vol. 29, No. 1, 73–82, 2025.

[27] Astuti, D. W., R. Rivayanto, M. Muslim, T. Firmansyah, D. A. Cahyasiwi, I. U. V. Simanjuntak, and Y. Natali, "Bandwidth enhancement for half mode substrate integrated waveguide antenna using defected ground structures," *International Journal of Electronics and Telecommunications*, Vol. 69, No. 3, 449–454, 2023.

[28] Setyawan, A., D. W. Astuti, M. Alaydrus, and Y. Wahyu, "Bandwidth enhancement of HMSIW antenna using half-octagonal ring slot," *J. Commun.*, Vol. 20, No. 2, 131–140, 2025.

[29] Jin, C., R. Li, A. Alphones, and X. Bao, "Quarter-mode substrate integrated waveguide and its application to antennas design," *IEEE Transactions on Antennas and Propagation*, Vol. 61, No. 6, 2921–2928, 2013.

[30] Pozar, D. M., *Microwave Engineering*, 4th ed., John Wiley & Sons, 2012.